# A Reaction Valley Investigation of the Cycloaddition of 1,3-Dipoles with the Dipolarophiles Ethene and Acetylene: Solution of a Mechanistic Puzzle

Thomas M. Sexton, Marek Freindorf, Elfi Kraka,[*,†] and Dieter Cremer[*,†]

[†]Computational and Theoretical Chemistry Group (CATCO), Department of Chemistry, Southern Methodist University 3215 Daniel Ave, Dallas, Texas 75275-0314, United States

Ⓢ *Supporting Information*

ABSTRACT: The reaction mechanism of the cycloaddition of 10 1,3-dipoles with the two dipolarphiles ethene and acetylene is investigated and compared using the Unified Reaction Valley Approach in a new form, which is based on a dual-level strategy, an accurate description of the reaction valley far out into the van der Waals region, and a comparative analysis of the electronic properties of the reaction complex. A detailed one-to-one comparison of 20 different 1,3-dipolar cycloadditions is performed, and unknown mechanistic features are revealed. There are significant differences in the reaction mechanisms for the two dipolarophiles that result from the van der Waals complex formation in the entrance channel of the cycloadditions. Hydrogen bonding between the 1,3-dipoles and acetylene is generally stronger, which leads to higher reaction barriers in the acetylene case, but which also facilitates to overcome the problem of a reduced charge transfer from 1,3-dipole to acetylene. Mechanistic differences are found in the prechemical and chemical reaction regions with regard to reactant orientation, preparation for the reaction, charge transfer, charge polarization, rehybridization, and bond formation. It is shown that similarities in the reaction barriers as determined by CCSD(T)-F12/aug-cc-pVTZ calculations result from a fortuitous cancellation of different electronic effects. In general, a caveat must be made with regard to oversimplified descriptions of the reaction mechanism based on orbital theory or energy decomposition schemes.
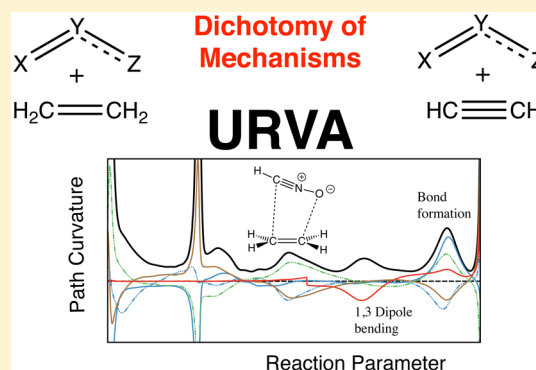
1. INTRODUCTION

The current investigation is part of a larger project aimed at designing catalytic reactions that proceed via a relatively low barrier to a desired product. In this connection, the Unified Reaction Valley Approach (URVA)[1−5] is used as a major tool. URVA in its 2016 version (URVA2016) provides an in-depth insight into the reaction mechanism beyond the results of any conventional quantum chemical analysis of the reaction mechanism.[6,7] Any new mechanistic method must verify its usefulness for a well-known set of reactions so that its advantages and disadvantages become transparent and well-understood. In this work, we chose 1,3-dipolar cycloadditions. Because of the large variation in the 1,3-dipoles XYZ (X, Y, Z: CHn; N, or O, X: NH or N; Y: CH$_2$, NH, or O) one expects a similarly large variation in the reaction mechanism.[8−12] Surprisingly, this expectation is not fulfilled, as the mechanism of all 1,3-dipolar cycloadditions is similar as was first proposed by Huisgen.[13] Huisgen pointed out the common nature of these cycloadditions as concerted pericyclic reactions, which, according to the Woodward–Hoffmann rules, should be symmetry-allowed ($\pi^4s + \pi^2s$)-reactions irrespective of the nature of the 1,3-dipole or the dipolarophile.[14−16] Although the concertedness of the 1,3-dipolar cycloadditions was heavily critiqued in the early days,[17] their basis nature as one-step reactions is generally accepted nowadays.[8−12]

Since the 1,3-dipolar cycloadditions are synthetically challenging,[18,19] provide the possibility of catalytic improvements,[20−23] and lead to desirable products,[24−27] investigations are in the hundreds and beyond what can be cited here. We focus in this work on the quantum chemical investigations, as they can provide a direct insight into the mechanism of the 1,3-dipolar cycloadditions.[28−40] Whenever the computational description of pericyclic reactions has to be considered, then the work of Houk and his co-workers deserves special mentioning, and this also holds for the 1,3-dipolar cycloadditions.[41−59] So far, the mechanism of these cycloadditions has been investigated from a general point of view,[52,60,61] where specific features such as the energetics,[48,53−55] kinetic aspects,[43] regio- and stereoselectivity,[28,30,36,47,62] concertedness,[40,45,46] or nonconcertedness in the presence of radical-stabilizing groups[44,50,63] are reported in the literature.

Those attempts deserve special attention, which analyze the reaction mechanism of the 1,3-dipolar cycloadditions with innovative tools such as the distortion energy of the reactants, which is supposed to rationalize trends in the observed

cycloaddition barriers,[41,42,49,51] the vibrational mode analysis of the reactants to find means for accelerating the reaction via mode enhanced reaction rates,[32,33,45,46] the investigation of the biradical character of the 1,3-dipoles to rationalize their reactive (dis)similarity,[29,31,42] or their potential zwitterionic character.[64] Finally, it has to be mentioned that comparative studies of Domingo and co-workers[65−67] are closely related to the current work, as they analyzed a similar set of reactions using however conventional tools of mechanistic quantum chemistry.

The mechanistic analysis presented in this work is off-mainstream insofar as it considers the whole reaction path and reaction valley from the early entrance channel where the van der Waals interactions between the reactants take place, to the late exit channel with the conformational adjustment of the products.[1−5] Any change in the direction of path and valley is registered by the URVA analysis and translated into the electronic structure changes causing the changes. In this way, URVA registers charge transfer, charge polarization, the adjustment between the reactants to adopt a suitable configuration, rehybridization at the reaction centers, and, most importantly, the processes of bond forming and bond breaking. Each of these mechanistic changes can be characterized by the adequate amount of energy needed, so that, based on the URVA analysis, individual contributions to the reaction barrier and reaction energy can be identified.[1−5] This analysis is meaningful because URVA provides the possibility of comparing different reaction paths directly to each other so that *mechanistic features of the 20 reactions investigated in this work can be presented in a single reaction diagram, which reveals in a simple way all (dis)similarities.* In addition to physically well-defined properties such as geometry, dipole moment, or polarizability, we included also properties based on model quantities such as natural bond orbital (NBO) charges, highest occupied molecular orbital−lowest unoccupied molecular orbital (HOMO−LUMO) gaps, which have been frequently used in the discussion of 1,3 dipolar reactions, although one must be aware of their shortcomings.[68,69]

Utilizing the advanced possibilities of URVA[3,7,70−74] this work will provide answers to a number of questions: (1) Why are the reaction barriers of ethene and acetylene cycloadditions so similar, while their reaction energies are so different? This is in contradiction with the Hammond−Leffler postulate, which predicts for the more exothermic reaction a lower barrier.[75,76] (2) What is the chemically decisive step of the reaction mechanism that determines the reaction barrier? (3) What influence have the van der Waals interactions in the entrance channel on the overall reaction mechanism and the energetics, or are these exclusively decided in the chemical phases? (3) Are there postchemical phases, and what influence do they have on the mechanism? (4) How are the bond-forming steps prepared, and what role does the mutual interaction between 1,3-dipole and dipolarophile play? (5) Is there a possibility to reduce the reaction barriers by including suitable substituents? (6) What general conclusions can be drawn based on the use of URVA2016 with its new features?

To answer these questions we investigate in this work the 1,3-dipolar cycloadditions between 10 different 1,3-dipoles (three diazonium betaines, three nitrilium betaines, three azomethines, and nitryl hydride; Figure 1) and the dipolarophile ethene. Next, we compare these reactions with the corresponding cyclo-additions involving acetylene as dipolarophile.[77] The results of this work are presented in the following way: Section 2 shortly summarizes the theoretical tools used in this work. Section 3 contains the results and discussions part where the latter focuses on a detailed description of the reaction mechanism. Section 4 compares the mechanism in dependence of the two dipolar-ophiles ethene and acetylene, whereas Section 5 draws the conclusions of the URVA analysis and discusses the chemical relevance of the current work.

2. COMPUTATIONAL DETAILS

The theoretical basis underlying URVA and the calculation of parameters along the path has been well-described in previous publications[3,6,70−73,77,78] and review articles.[1,2,4,5] Of particular interest to this investigation is the previous study of the reactions of 1,3-dipoles with acetylene.[77]

URVA follows the reaction complex (RC) along the reaction path through the reaction valley in $(3N − L)$-dimensional space (N: number of atoms of RC; L: number of translations and rotations) from reactants to products via the transition state (TS) utilizing mass-weighted coordinates. Any change in the electronic structure of the RC is registered by its vibrations, and any change in the vibrations leads to a change in the coupling with the translation along the path.[79] URVA determines these changes by the curvature coupling coefficients $B_{\mu,s}$ (μ denotes the vibration; s denotes the position along the path in terms of its arc length). The curvature coupling coefficients determine the scalar curvature $\kappa(s)$ given as the length of the curvature vector κ, which measures the curving of the path.[4,5,79] Hence, any change in $\kappa(s)$ reflects a specific electronic structure change of the RC, which is analyzed in URVA2016 by a decomposition of the curvature in terms of local *internal coordinate modes* that have been defined recently.[6] These modes (henceforth, called curvature compo-nents) characterize the electronic structure changes in terms of its magnitude (importance) and position along the reaction path. In this way bond breaking (forming), charge transfer, rehybridization, etc. can be located and described in detail. The new decomposition into internal coordinate modes has turned out to be robust in the case of reactions with biradical/biradicaloid character to which the 1,3-dipolar reactions belong.[31] The single-reference description of reactions having an amount of biradical/biradicaloid character may lead to reaction path instabilities (denoted by imaginary frequencies in the reaction valley). A reaction path curvature decomposition into local or normal mode contributions tends to fail in such a situation. The decomposition into internal coordinate modes described by Zou and co-workers[6] and implemented in URVA2016 avoids this failure, even in the case of reactions characterized by strong multireference character.[6]

Changes in energy, geometry, path direction, scalar curvature of the path, atomic charges, charge transfer, dipole moments, isotropic polarizability, and other variables are routinely monitored as a function of the path length s. The mechanism is dissected into reaction phases, which are defined by the minima of the scalar curvature $\kappa(s)$ and given as M1, M2, etc. starting in the entrance channel of the reaction valley ($s < 0$; $s(TS) = 0$ amu$^{1/2}$/bohr, henceforth called s-units). A curvature enhancement or peak indicates electronic structure changes, whereas a curvature minimum is normally indicative of a lower activity of the RC typically happening between two different electronic structure changes. However, there are also situations in which two electronic structure changes couple, so that a curvature peak is characterized by a shoulder caused by the second process. It is useful to consider such a curvature shoulder as belonging to a new reaction phase. The phase borders can be defined in this case by the component analysis of the path direction.
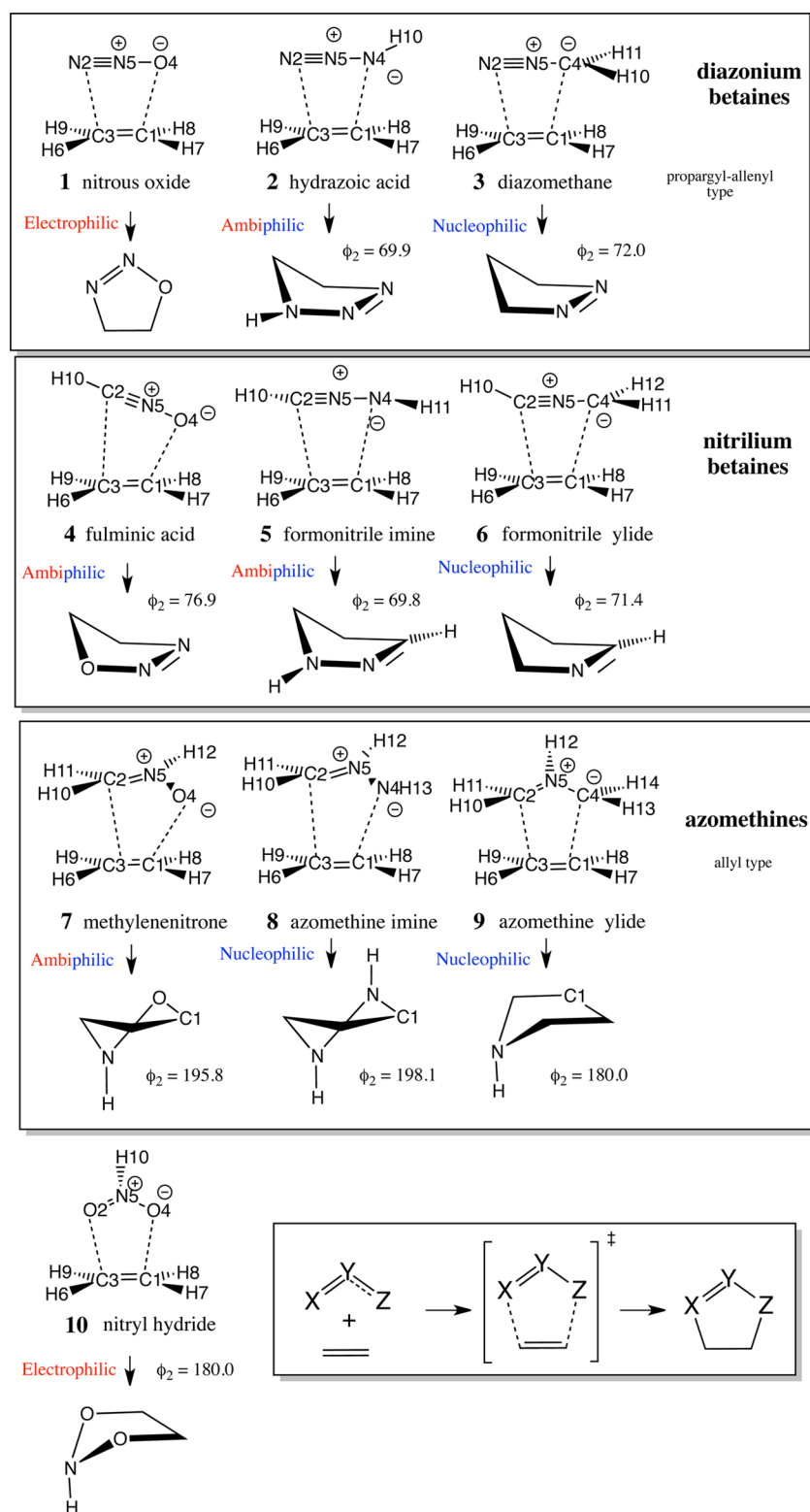
Figure 1. 1,3-Dipolar cycloaddition systems **1−10** investigated in this work. The conformation of the product is given in terms of puckering coordinates[81,83,84] to quantify differences in the puckering. The phase angle ϕ_2 depends on the numbering of the ring: clockwise starting at Y.

Using URVA2016 and an improved path-following algorithm,[80] the reaction valley can be followed far out into the van der Waals region of entrance and exit channel in steps of 0.03 s units thus leading to 1000 and more path points at which energy, first-, second-, and third-order response properties are calculated.[6] In this connection, it has turned out to be useful to distinguish between prechemical, chemical, and postchemical reaction phases.[7]

In the prechemical phases the reaction partners orient to each other. In the chemical phases, the chemical processes take place, whereas in the postchemical phases the product adopts the equilibrium conformation.

In addition to an analysis of the curvature in terms of bond length, bond angle, and dihedral angle components, we also used conformational components such as pyramidalization and

Table 1. Energetics of Cycloaddition Reactions 1−10[a]

reaction	$\Delta_R E$ ωB96X-D e	$\Delta_R E$ ωB96X-D a	$\Delta_R E$ B3LYP e	$\Delta_R E$ CCSD(T)-F12a e	ΔE^a ωB96X-D e	ΔE^a ωB96X-D a	ΔE^a B3LYP e	ΔE^a CCSD(T)-F12a e	$\Delta_R H$ CCSD(T)-F12a e	ΔH^a CCSD(T)-F12a e	$\Delta_R S$ ωB97X-D e	ΔS^a ωB97X-D e	$\Delta_R G$ CCSD(T)-F12a e	ΔG^a CCSD(T)-F12a e
1 (NNO)	−9.1	−42.3	−8.8	−10.0	29.8	27.5	24.9	26.8	−7.3	27.2	−34.6	−35.0	3.0	37.6
2 (NNNH)	−26.7	−67.7	−23.8	−26.9	22.4	19.7	18.9	19.3	−22.8	20.3	−41.9	−37.9	−10.3	31.6
3 (NNCH$_2$)	−38.6	−56.8	−34.7	−40.3	16.6	14.3	15.8	13.1	−35.6	14.2	−42.4	−37.7	−23.5	25.4
4 (HCNO)	−46.2	−82.0	−43.6	−47.2	15.2	12.9	12.8	11.3	−43.1	11.9	−39.0	−35.2	−31.5	22.4
5 (HCNNH)	−66.3	−107.9	−60.4	−65.7	8.8	7.7	8.2	6.1	−60.5	6.9	−41.6	−37.2	−47.6	18.0
6 (HCNCH$_2$)	−76.4	−95.3	−69.7	−77.1	7.3	6.3	8.4	4.3	−71.8	5.2	−42.8	−37.8	−59.0	16.4
7 (H$_2$CNHO)	−35.3	−50.3	−31.5	−35.6	14.1	13.3	13.4	12.5	−31.5	13.5	−41.8	−39.9	−19.1	25.4
8 (H$_2$CNHNH)	−52.7	−66.4	−45.6	−51.5	8.3	7.0	9.3	6.6	−47.0	7.7	−39.7	−39.7	−35.2	19.6
9 (H$_2$CNHCH$_2$)	−71.7	−84.7	−64.8	−71.0	0.9	1.1	3.4	~0	−65.9	1.0	−39.6	−38.0	−54.1	12.3
10 (ONHO)	−9.1	−22.1	−7.5	−10.5	31.1	31.1	27.1	28.7	−7.2	29.6	−39.5	−39.1	4.6	41.2

[a]Energetics of cycloaddition reactions 1−10 involving ethene (e) or acetylene (a). Values for acetylene from ref 77. B3LYP calculations performed with the 6-31G(d,p) basis set. Reactant energies are BSSE corrected. All other calculations were performed with the aug-cc-pVTZ basis set. Enthalpies and free energies were obtained with ωB97X-D geometries and thermochemical corrections. $\Delta_R E$, $\Delta_R H$, $\Delta_R G$, $\Delta_R S$ correspond to the reaction energy, enthalpy, free energy and entropy; ΔE^a, ΔH^a, ΔG^a, ΔS^a correspond the activation energy, enthalpy, free energy and entropy. (Energy differences in kcal/mol and entropy differences in cal/(mol K)).

puckering coordinates for the description of the path curvature. Since five-membered rings are formed in reactions 1−10 and some of these are puckered, we utilized the Cremer−Pople puckering coordinates for the conformational description.[81−84] For the purpose of quantitatively assessing the degree of rehybridization during the cycloaddition reaction, the curvature was also characterized in terms of pyramidalization angle components for the CH$_2$ groups defined by the deviation of all C(sp^2) bonds from planarity ($\tau = 0°$) and adopting tetrahedral angles in the ideal case of an sp^3-hybridized CH$_2$ group (τ(max) = 19.5° or another value depending on the structure of the reactant). The value of $(\tau$(max) − $\tau(s))/\tau(s)$ given in percentage gives the degree of rehybridization at a path point s. Similarly, the bending of acetylene caused by the 1,3-dipolar cycloaddition can be expressed where a direct comparison of the rehydridization of ethene and acetylene is possible, because reaction path and valley are described in mass-weighted coordinates. *It is an important advantage of the URVA analysis that different reactions can be directly compared,* which otherwise would only be possible for the stationary points on the potential energy surface (PES).

All reactions of this study are examined by a dual-level approach. The energetics is determined with a high-level approach in form of coupled cluster with all single and double excitations and a perturbative treatment of the triple excitations plus an explicit electron correlation with the F12 excitation operator (CCSD(T)-F12).[85,86] The reaction valley and reaction path are analyzed with URVA employing a less costly method in the form of B3LYP.[87,88]

In additional complete active space self consistent field calculations, we performed the URVA analysis for some of the cycloadditions (6, 9, 10) and compared its results with those obtained with the density functional theory (DFT) hybrid functionals. The mechanistic description in form of the curvature decomposition diagrams does not change, which is an observation that we have made repeatedly in our URVA studies and which we could trace back to the self-interaction error of the XC functionals being used. DFT includes left−right electron correlation effects resulting from the exchange self-interaction error[89−92] and therefore accounts for some of the multireference effects. This is the reason why only a few path instabilities due to multireference effects are found for the reaction systems investigated. As described by Zou and co-workers,[6] these path

instabilities no longer cause a problem for the URVA analysis. Besides the B3LYP hybrid functional, the influence of possible dispersion errors was investigated by performing ωB97X-D calculations.[93] The latter is known to lead to geometries and relative energies close to CCSD(T) values.[94] These calculations as well as those at the CCSD(T)-F12a level of theory[86] were performed with Dunning's aug-cc-pVTZ basis set.[95] Thermochemical corrections obtained at the ωB97X-D/aug-cc-pVTZ level of theory were used to calculate the energetics of the 20 reactions in terms of relative enthalpies and relative free energies at the CCSD(T)-F12/aug-cc-pVTZ level of theory. Charge transfer and charge polarization of the RC when moving along the reaction path were calculated using the NBO analysis of Weinhold and co-workers.[96,97] All URVA-related properties were found with the program package COLOGNE16.[98] For the coupled cluster calculations the program MOLPRO[99] was used, whereas the DFT calculations were performed with Gaussian09.[100]

3. RESULTS AND DISCUSSION

The energetics of the reactions investigated in this work is analyzed and compared with that of the corresponding acetylene reactions in Tables 1 and 2. Calculated electrical properties (dipole moments and polarizabilities) of the RCs 1−10 are listed in Table 3, while in Table 4 properties of the two dipolarophiles ethene and acetylene are listed.[101,102] The formation of (bi)radicaloids precedes bond formation. The data in Table 5 describe the rehybridization of the reactants to form the (bi)radicaloids and gives the asynchronicity of the cycloaddition reactions.

Reaction Energetics. The first three 1,3-dipole reactions involve the diazonium betaines XYZ (propargyl-allenyl type 1,3-dipoles; XY: N≡N, Z: O, NH, CH$_2$) 1, 2, and 3 that lead to relatively high barriers at the CCSD(T)-F12 level of theory (26.8, 19.3, and 13.1 kcal/mol, Table 1 and Figure 1) and moderate exothermicity ($\Delta_R E$: −10.0, −26.9, and −40.3 kcal/mol). Reactions 4, 5, and 6 have as a 1,3-dipole a nitrilium betaine (XY: HC≡N, Z: O, NH, CH$_2$), which leads to more exothermic reactions ($\Delta_R E$: −47.2, −65.7, −77.1 kcal/mol) and lower barriers (11.3, 6.1, 4.3 kcal/mol). Finally, three allyl-type 1,3-dipoles were reacted with ethene: The azomethines 7, 8, and 9 (allyl-type

Table 2. Energy Changes for Regions of the Reaction Path for Ethene and Acetylene[a]

reaction	ΔE(vdW) e	ΔE(vdW) a	ΔE[a] e	ΔE[a] a	ΔE(prep) e	ΔE(prep) a	ΔE(bend) e	ΔE(bend) a	ΔE(bond 1) e	ΔE(bond 1) a	ΔE(bond 2) e	ΔE(bond 2) a	ΔE(exit) e	ΔE(exit) a
1 (NNO)	0.01	−0.34	24.9	24.7	1.20	1.07	23.7	23.6	−27.9	−63.3	−5.8	−8.3	−33.7	−71.6
2 (NNNH)	−2.49	−1.74	21.2	19.4	4.57	2.60	16.7	16.7	−32.5	−48.7	−10.2	−39.7	−42.7	−88.4
3 (NNNCH₂)	0.63	−0.87	15.2	16.0	1.16	1.67	14.1	14.3	−48.4	−68.6	−2.0	−3.3	−50.4	−71.9
4 (HCNO)	−0.33	−1.74	13.2	14.9	2.60	3.99	10.6	11.1	−52.0	−87.4	−4.4	−10.4	−56.4	−97.7
5 (HCNNH)	−1.45	−2.55	9.3	10.6	3.28	3.21	6.0	7.5	−61.8	−97.8	−6.8	−19.4	−68.6	−117.3
6 (HCNCH₂)	−0.14	−2.44	8.5	11.3	2.14	3.98	6.4	7.4	−61.0	−78.6	−17.0	−23.8	−78.0	−102.4
7 (H₂CNHO)	−0.99	−3.23	14.4	16.4	4.08	6.29	10.3	10.1	−40.0	−49.5	−4.9	−14.8	−44.9	−64.3
8 (H₂CNHNH)	−2.59	−4.77	11.6	13.3	4.65	6.26	7.0	6.9	−48.5	−60.3	−6.4	−13.8	−54.9	−74.1
9 (H₂CNHCH₂)	0.96	−0.66	2.4	2.8	0.57	0.15	1.9	2.7	−55.0	−58.1	−13.2	−28.9	−68.2	−86.9
10 (ONHO)	−3.66	−3.88	30.5	29.9	9.19	6.05	21.4	23.8	−26.6	−31.7	−7.9	−19.5	−34.5	−51.1

[a]Energy changes for regions of the reaction path (in kcal/mol). Included are columns for: ΔE(vdW) (van der Waals complexation energy, the energy of the RC on the first path point (minimum), values are BSSE corrected); Activation energy ΔE[a]: E change from start of path to TS; ΔE(prep): E change from start of path to beginning of the first chemical phase, (e.g., energy consumed during the prechemical phases); ΔE(bend): E change from start of bending phase to TS; ΔE(bond 1): E change from TS to end of first bond phase; ΔE(bond 2): E change from end of first bond phase to end of path, and ΔE(exit): E change from TS to end of path. If a van der Waals complex is formed (negative ΔE(vdW)), the energy change from the start of the path to the TS is larger than the activation energy given in Table 1 as there the TS energy is compared to the energy of the separated reactants. B3LYP/6-31G(d,p) calculations.

Table 3. Properties of 1,3-Dipoles and Reaction Complexes 1−10 Reacting with Ethene[a]

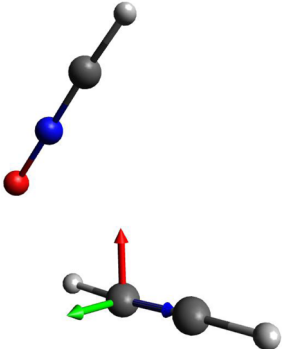| reaction	polarizability α α_{xx}	α_{yy}	α_{zz}	α_{iso}	dipole moment μ μ_x	μ_y	μ_z	μ_{total}	orien- tation
1	1.1	1.1	4.1	2.1	0	0.01	−0.01	0.01	7.3
2	1.5	1.5	5.4	2.8	1.15	1.17	1.07	1.96	−1.1
3	2.3	1.6	6.4	3.4	0.00	0.20	1.71	1.72	−10.0
4	1.3	1.7	5.1	2.7	0.00	0.89	−3.00	3.13	34.2
5	1.9	2.0	7.2	3.7	1.38	−1.25	0.89	2.06	2.7
6	2.6	2.3	8.7	4.5	0.00	1.31	0.98	1.63	−13.9
7	3.0	2.3	5.0	3.4	1.09	1.83	−2.69	3.43	27.5
8	3.7	1.8	6.9	4.1	0.31	0.47	−2.26	2.33	9.4
9	3.9	2.0	9.0	5.0	−1.23	0.59	0	1.36	0.0
10	1.8	1.3	3.5	2.2	−2.46	0.82	0	2.60	0.0

[a]Reference point is **C**, that is, the first point of the last prechemical phase. Dipole moment components μ_α (α = x, y, z) and total dipole moment μ_{total} (in debye); polarizability components $\alpha_{\alpha\alpha}$ and isotropic polarizability α_{iso} (in Å³); orientation angle of the 1,3-dipole (X2Z4 axis) relative to the CC axis of ethene. B3LYP/6-31G(d,p) calculations with regard to the isolated 1,3-dipole in the geometry of the reaction complex at point **C**. See Table 4 for axis definitions.

1,3-dipoles; XY: H₂C=NH, Z: O, NH, CH₂) lead to reaction energetics similar to those of the nitrilium betaines ($\Delta_R E$: −35.6, −51.5, −71.0 kcal/mol; ΔE[a]: 12.5, 6.6, ~0 kcal/mol), whereas the reaction energetics of nitryl hydride 10 resembles that of the diazonium betaines ($\Delta_R E$: −10.5; ΔE[a]: 28.7 kcal/mol). These trends are correctly reproduced by the two XC functionals used in this work (Table 1).

A comparison of the energetics of the ethene reactions with those of the acetylene reactions (Table 1) reveals that the latter are always more exothermic (16−41 kcal/mol for the diazonium betaines; 18−42 kcal/mol for the nitrilium betaines, and 12−15 kcal/mol for the allyl-type 1,3-dipoles, Table 1). The larger exothermicity in the case of acetylene is clearly a result of the fact that planar π-delocalized (partially aromatic) products are formed, whereas in the ethene reactions puckered five-membered rings are generated that do not benefit from π-delocalization. According to the Hammond−Leffler postulate,[75,76] more exothermic reactions should have an earlier TS and a lower barrier. This is not confirmed for the acetylene reactions, which are more exothermic but have always larger barriers if these are determined with regard to the separated reactants at the CCSD(T)-F12/aug-cc-pVTZ level of theory (Table 1).

The reactants can form van der Waals complexes, which prefer an end-on H-bonded rather than π-complex configuration (exceptions: 1, 9, and 10) and are more stable than the corresponding ethene complexes (Figure 2 and Table 2). The failure of the Hammond−Leffler postulate becomes understandable if one compares the energy profiles of the ethene and acetylene reaction. These are characterized by differently long prechemical regions and little similarity between the ethene and acetylene starting geometries. Also, the products have different geometries (planar in the first case and puckered in the second). Hence, an important prerequisite of the Hammond−Leffler postulate (similarity in the structures of TS and reactants/products) is not fulfilled.[75,76]

Houk and co-workers[49,51] have argued that the similarity in the barriers results from the fact that the barriers are dominated by the distortion of the 1,3-dipole. These authors point out that the distortion of acetylene requires somewhat more energy thus leading to the small difference in the barriers. Cossio and co-workers,[103,104] who examined reactions 4 and 7 with acetylene and with ethene, suggested that the TS of **4a** (a: acetylene) establishes a π aromatic system. However, the π aromaticity measured by nucleus-independent chemical shifts (NICS) is

Table 4. Comparison of Acetylene and Ethene[a]

dipolarophile	α_{zz} [Å³]	α_{yy} [Å³]	α_{xx} [Å³]	α_{iso} [Å³]	
ethene	4.61	1.32	3.07	3.00	
acetylene	4.17	1.19	1.19	2.18	
	HOMO [Hartree]	LUMO [Hartree]	LUMO−HOMO [Hartree]	k^a [mdyn/Å]	ω^a [cm⁻¹]
ethene	−0.374 46	0.182 79	0.557 25	1.63	968
acetylene	−0.404 43	0.220 22	0.624 65	0.15	624
	IP [eV]	EA [eV]	IP-EA [eV]	R(CC) [Å]	ref
ethene	10.5	−1.5	12.0	1.330	101,102
acetylene	11.5	−2.5; −1.8	14.0; 13.3	1.205	101,102

[a]Polarizabilities, C−C bond lengths, local mode force constants k^a, and local mode vibrational frequencies ω^a calculated at B3LYP/6-31G(d,p). HOMO and LUMO energies at HF/6-31G(d,p). The z axis, shown in blue, points along the dipolarophile CC bond. The y axis, shown in red, points in the π direction of the dipolarophile, toward the incoming 1,3-dipole. The x axis, shown in green, lies perpendicular to the y and z axes. The x axis lies in the plane of ethene.

Table 5. Differences in Rehybridization of 1,3-Dipole and Dipolarophile as Determined by the Reaction Path Curvature[a]

reaction	Δs(acetylene)	Δs(ethene)	difference $\Delta\Delta(s)$	asynchronicity acetylene	asynchronicity ethene
1 (NNO)	−0.57	−1.71	1.14	22.6	16.2
2 (NNNH)	−0.99	−1.92	0.93	9.2	3.2
3 (NNNCH₂)	−0.12	−1.35	1.23	−21.9	−15.5
4 (HCNO)	−0.45	−1.68	1.23	41.3	22.7
5 (HCNNH)	−0.45	−1.62	1.17	28.0	13.7
6 (HCNCH₂)	−0.36	−1.29	0.93	−8.4	0.1
7 (H₂CNHO)	0.12	−0.69	0.81	23.7	16.7
8 (H₂CNHNH)	1.05	−0.69	1.74	17.1	11.4
9 (H₂CNHCH₂)	0.09	−0.75	0.84	0.0	0.0
10 (ONHO)	0.30	−0.15	0.45	0.0	0.0

[a]The rehybridization delay Δs gives the shift of the curvature peak due to 1,3-dipole bending into the entrance channel relative to the minimum of the C3 (or C1) bending/pyramidalization component of the reaction path curvature (compare with Figure 3, first chemical phase; there, Pyr denotes pyramidalization). Negative values indicate the 1,3-dipole bending occurs before the rehybridization of the dipolarophile. Difference $\Delta\Delta s$ measures the delay in ethene pyramidalization relative to C3 (C1) bending. The asynchronicity in bond formation is derived from the offset of the rehybridization processes expressed in percentage. Path positions s and Δs values are given in amu$^{1/2}$bohr (s units). B3LYP/6-31G(d,p) calculations.

similar for the TS of **4e** and that of **4a**. (If the ethene reaction has to be distinguished from the acetylene reaction the symbols **4e** and **4a** are used.) These authors concluded that only *in-plane* aromaticity is significant in these TSs, and the fact that the acetylene products are aromatic does not indicate that acetylene TSs will benefit from extra aromatic stabilization. Domingo and co-workers[65] investigated a similar set of 1,3-dipolar cyclo-additions for ethene and acetylene. They mention that the geometry of the RC involving acetylene is more asynchronous at the TS than in the case of ethene. One could speculate that with increasing asynchronicity the barrier increases, but this depends

on whether bond formation is before (increase of the barrier) or after (decrease of the barrier) the TS. Apart from this, Domingo and co-workers treat the barriers for the two dipolarphiles as equal and try to predict them via the electrophilicity (nucleophilicity) and chemical hardness of the 1,3-dipole.[65,66]

We will show in the following that these arguments might not be relevant for the peculiar energetics of reactions **1−10**. In Figure 3a−j, the curvature diagrams for the 10 ethene reactions investigated are displayed. The scalar curvature is given by the bold black line, and the most important curvature components are shown in colored lines.
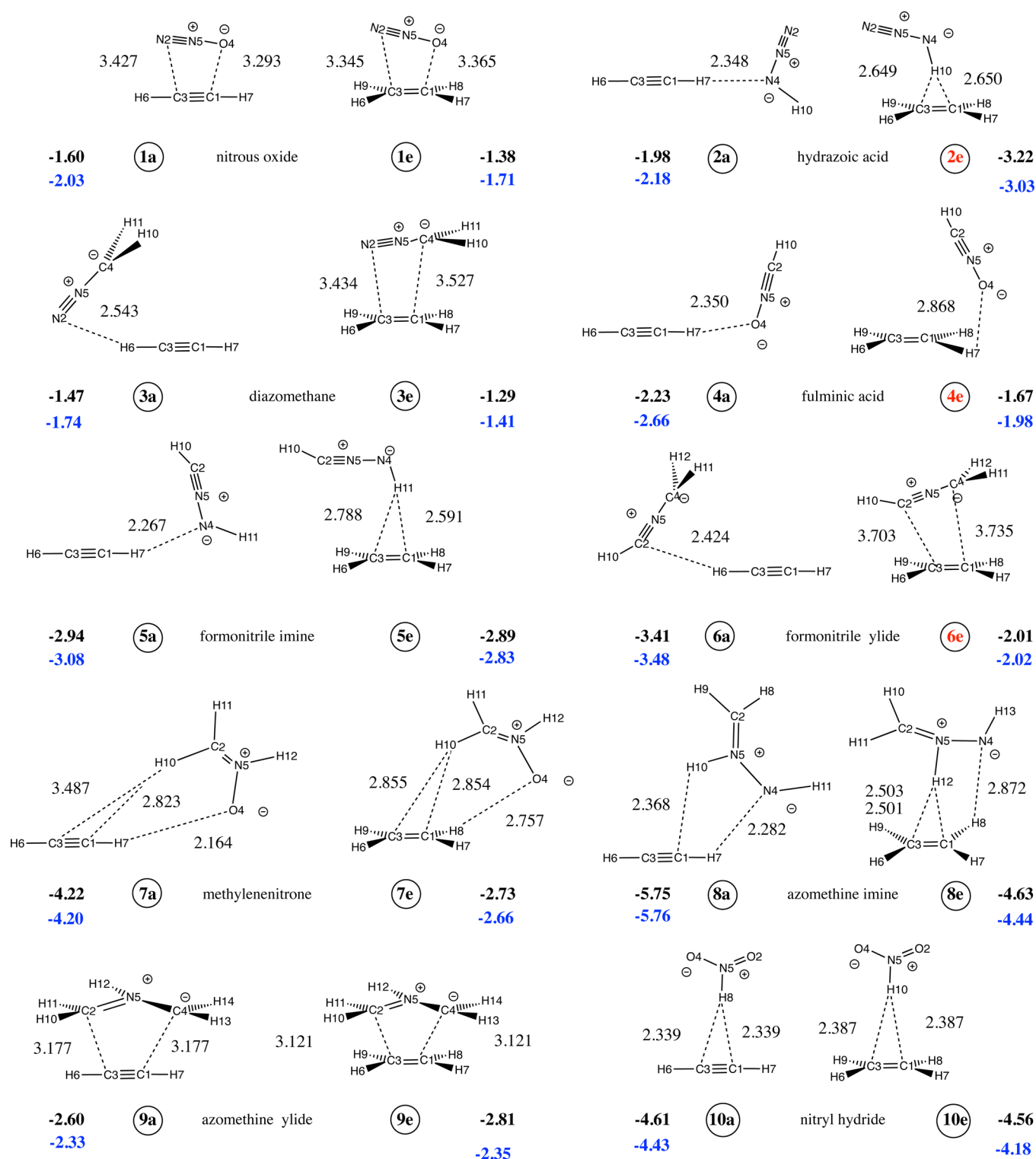
Figure 2. van der Waals complexes for **1a–10a** and **1e–10e** as calculated at the ωB97X-D/aug-cc-VTZ level of theory (black numbers) or at CCSD(T)-F12/aug-cc-pVTZ (blue numbers). Schematic presentation of the H interactions by dashed lines with distances in Å. Bold numbers give BSSE-corrected binding energies relative to the separated reactants. Note that in several cases rotations out of plane are needed to perform the cycloaddition.

Reaction Mechanism. As in the case of the acetylene reactions,[77] a three-phase mechanism is found for the 1,3-dipolar cycloadditions of ethene in the chemical region. The mechanism involves a bending (rehybridization) phase in the entrance channel (before or containing the TS at 0 s units) and a bond-forming phase for the first and another one for the second bond in the exit channel. The three chemical phases (gray areas in Figure 3a–j)

are preceded by up to four prechemical phases, in which the reaction partners orient to each other. The energy requirements for the orientation are in the range of 0.6−4.6 kcal/mol (see Table 2) with the exception of reaction **10**. For nitryl hydride the correct orientation requires 9.2 kcal/mol, which is understandable in view of the synchronicity of the bond-forming step. In the following the curvature diagrams of the prechemical phases will
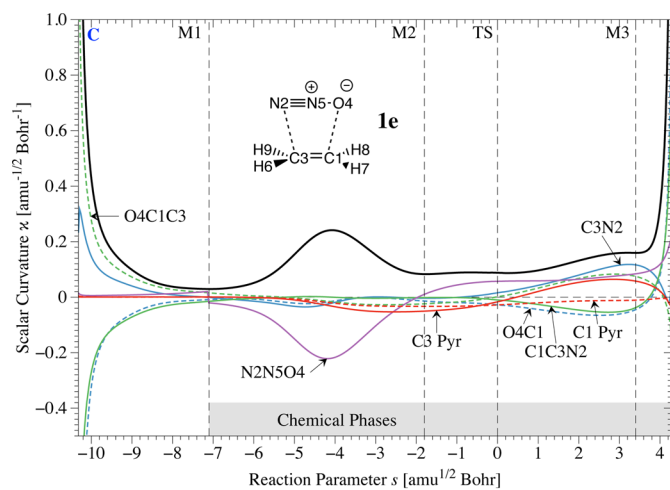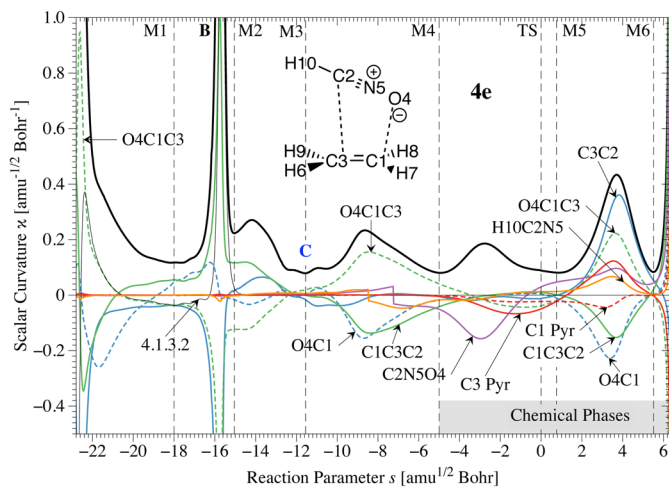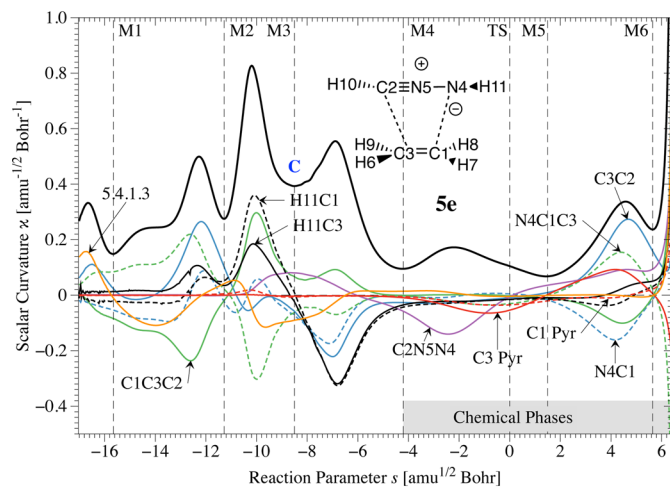
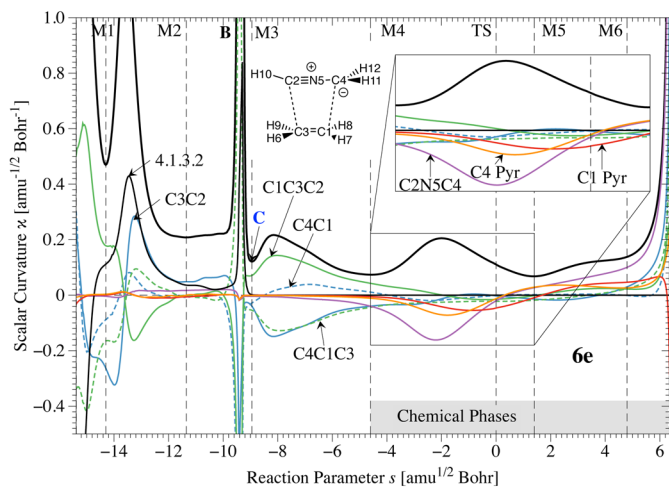(a) **1**: Nitrous oxide + Ethene
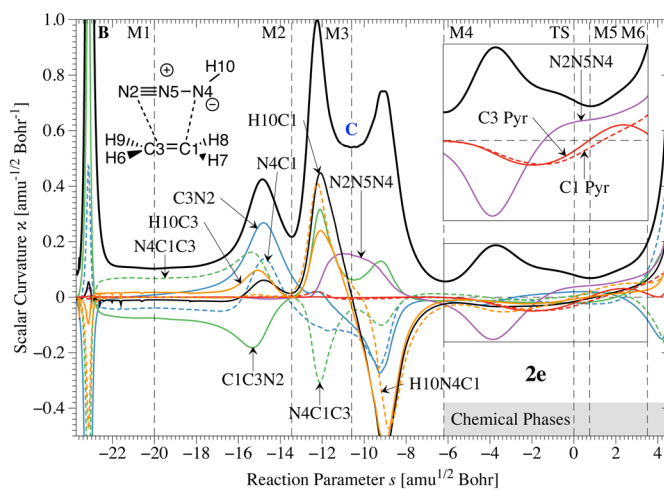
(b) **2**: Hydrazoic acid + Ethene
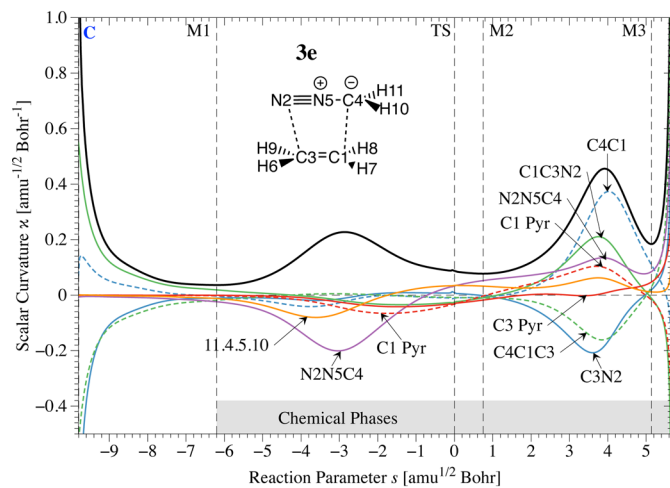
(c) **3**: Diazomethane + Ethene

(d) **4**: Fulminic acid + Ethene

(e) **5**: Formonitrile imine + Ethene

(f) **6**: Formonitrile ylide + Ethene

Figure 3. continued

(g) **7**: Methylenenitrone + Ethene

(h) **8**: Azomethine imine + Ethene

(i) **9**: Azomethine ylide + Ethene
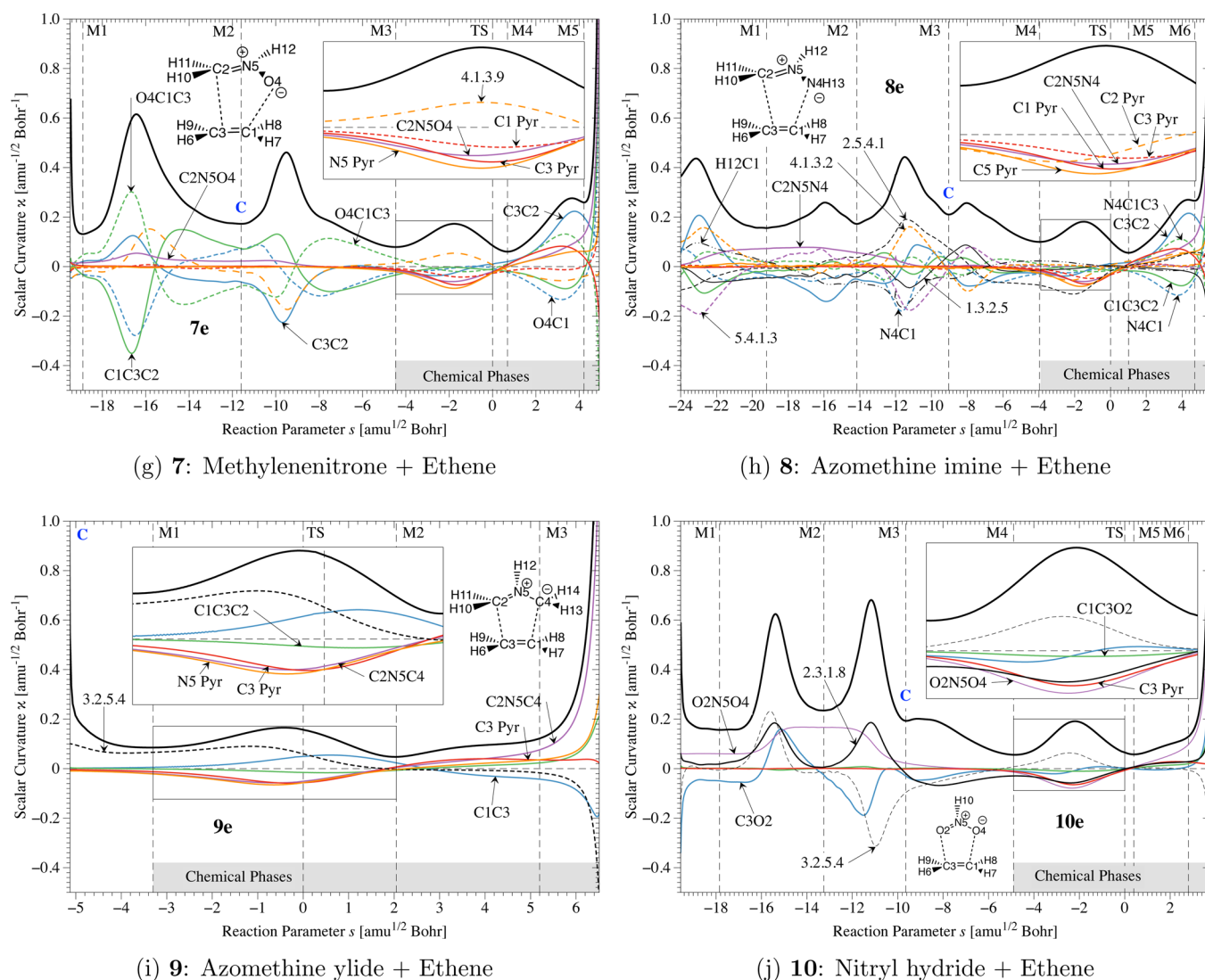

(j) **10**: Nitryl hydride + Ethene

Figure 3. Scalar curvature as a function of the reaction path parameter s (solid black line) for 1,3-dipolar cycloadditions **1−10**. Decomposition of the scalar curvature into components is given in color. The borders of the reaction phases are indicated by vertical dashed lines at curvature points M1, M2, M3, etc. The TS at $s = 0$ amu$^{1/2}$ bohr is also indicated by a vertical dashed line. Curvature peaks due to bifurcation points are marked by **B** in the entrance channel for reactions **2**, **4**, and **6**. Point **C** denotes the beginning of the last prechemical phase at which some of the RCs adopt coplanarity (see text). B3LYP/6-31G(d,p) calculations.

be discussed for the purpose of clarifying how the cycloaddition is initiated, and the RC is prepared for the chemical phases.

Pre-Chemical Phases. All cycloadditions are initiated by the formation of a van der Waals complex, where stabilities vary between 1.41 and 5.76 kcal/mol according to basis set super-position error (BSSE)-corrected CCSD(T)-F12/aug-cc-pVTZ calculations (Figure 2; somewhat smaller binding energies are obtained with B3LYP/6-31G(d,p); Table 2). Several of the van der Waals complexes are stabilized by dipole−induced dipole interactions (**1a**, **1e**, **3e**, **6e**), others by H-bonding involving the acetylene or ethene H atoms and a heteroatom (**2a**, **3a**, **4a**, **4e**, **6a**), again others by nonclassical CH⋯π interaction (**2e**, **5e**, **10a**, **10e**), or by both classical H-bonding and nonclassical H⋯π interactions (**7a**, **7e**, **8a**, **8e**). Dispersion is most probably contributing to the stability of complexes **6e**, **9a**, and **9e** as the 1,3-dipoles possess high isotropic polarizabilities (see, e.g., Table 3). For each complex, the electrostatic nature of the interactions can be enhanced by small covalent contributions provided orbital overlap and sufficient charge transfer from electron donor to electron acceptor can take place.

It is noteworthy that most van der Waals complexes are more stable in the case of acetylene. This is the result of a more acidic CH bond in acetylene, which leads to somewhat stronger electrostatic interactions (exception: **9e** is dominated by dispersion; Figure 2). The larger stability of the acetylene van der Waals complexes is also confirmed at the CCSD(T)-F12/aug-cc-pVTZ//ωB97X-D/aug-cc-pVTZ level of theory (see Figure 2). The analysis of the van der Waals complexes shown in Figure 2 leads two important conclusions: (i) The more stable van der Waals complexes should increase the cycloaddition barrier in the case of the acetylene reactions and (ii) There should be a large variety in the mechanism of the cycloaddition reactions considering the different van der Waals configurations. Hence, the similarity in the reaction barriers and the reaction mechanism can hardly be understood in view of the different exothermicities and the different starting configurations of the RC (Figure 2).

Before resolving this obvious dichotomy of mechanistic findings, another peculiarity of the prechemical phases must be

discussed. In the entrance channel of reactions **2e**, **4e**, and **6e**, unusually large and narrow curvature peaks indicate the appearance of a reaction path bifurcation point (**B**),[6,7] where C_1-symmetrical RCs adopt a higher symmetry required for a maximal overlap between the π-systems of 1,3-dipole and dipolarophile. For example, in the case of **4e**, point **B** is positioned at $-16\ s$ units. The first phase of **4e** is characterized by a stabilizing O4···H7 interaction. In the second orientation phase, which contains the **B** point, the O···H interaction is weakened, and O4 becomes centered over C1 so that a C_s-symmetrical RC is formed (Figure 3d). Similarly, **B** in **2e** corresponds to a rotation of the N−H bond either clockwise or counterclockwise out of the heavy atom plane, whereas in **6e** a rotation of ethene leads either to the envelope form at $\phi_2 = 71.4°$ or the inverted form at $71.4 + 180 = 251.4°$ (rotation of C3C1 at a hypothetical C3C2 axis into or out of the drawing plane in Figure 2). Within the URVA description, the symmetry of the RC can only be changed at a stationary point such as **B**.[105,106] **B** points are possible for some of the ethene reactions but are not found for the acetylene reactions.

Orientation and Breaking the Intermolecular Hydrogen Interactions. Stabilizing van der Waals interactions involving CH bonds must be cleaved to obtain the RC configuration required for the pericyclic reaction. At least one or both reactants within the RC need to rotate so that they can carry out the suprafacial attack of the 1,3-dipolar cycloaddition. This leads in the case of the RCs with nonclassical H-π interactions (**2e**, **5e**, **7e**, **7a**, **8e**, **8a**, and **10e**) to a curvature pattern including three or four prechemical phases. The first two phases (start to M2; see Figure 3b,e,g,h,j) are dominated by the rotation of the reactants initiating the H-bond breakage. This is reflected by the fact that the curvature peaks in these phases are dominated by curvature components involving the intermolecular angles C1C3X2 and C3C1Z4 or dihedral angles such as Z4C1C3X2.

Phases 3 and 4 are characterized by curvature components associated with the H-bond interactions (see, e.g., Figure 3b,e). Because of the rotation of the reaction partners the H-bonding interactions are broken as reflected by resisting (negative) H-bond curvature components. Phases 3 and 4 are also characterized by a start of the bending of the 1,3-dipole as reflected by a positive XYZ component, for example, N2N4N5 in the case of **2e**. If the reactants can approach each other in coplanar (heavy atom) plane as in the case of **1**, **3e**, or **9**, the prechemical region consists of just one phase that corresponds to an in-plane reorientation from the van der Waals complex to an RC with decreasing CX and CZ distances (see Figure 3a,c,i).

Table 2 reveals that the energy needed in the prechemical phase(s) to transform the van der Waals complex into a form ready for cycloaddition varies from 4 (no H interactions) to 47% of the reaction barrier, where the dipolarophile acetylene mostly leads to stronger van der Waals complexes and therefore requires up to 10% more energy than the dipolarophile ethene. The differences in the energies required in the prechemical cases are parallel to the differences in the reaction barriers (Table 2) with the exception of systems **5** and **9**. This is remarkable but does not explain the similarities in the reaction barriers, which are in clear contradiction to the Hammond−Leffler postulate (the more exothermic reactions with acetylene should lead to lower rather than higher barriers). The following investigation of the chemical phases will reveal that the situation is more complicated.

Polarization and Charge Transfer. All 1,3-dipolar cycloadditions require the coplanar arrangement of the reactants, which requires configurational changes of the RC (rotation of the reactants relative to each other) and/or the breaking of hydrogen interactions. Coplanarity is a prerequisite for an effective charge transfer from the 1,3-dipole to the dipolarophile, which is accompanied by a mutual polarization of the reactants. Four properties of the reactants determine polarization and charge transfer: (i) Exchange repulsion between the reactants as determined by their *exchange repulsion envelopes*;[107] (ii) Dipole-induced dipole interactions as related to the magnitude and orientation of the dipole moment μ of the 1,3-dipole (provided there is one) and to (iii) the polarizability of the reactants as measured by the polarizability tensor $\boldsymbol{\alpha}$ and the isotropic polarizability α_{iso}; (iv) Charge transfer ability of each reactant as determined by overlap and energy of the frontier orbitals.

Coplanarization is finalized in the prechemical phase before the chemical processes start. There, the approach distances between the atoms forming the new bonds can be considerably different. For reaction **4e**, C1O4 = 3.266 Å and C3C2 = 4.165 Å, which is contrary to the fact that the C3C2 bond will be formed first. At this stage of the reaction, the approach distances reflect differences in the exchange repulsion interactions between the reactants. For asymmetric dipoles like **4**, the electron density of the more electronegative O4 is more contracted than the electron density of C2, thus leading to a smaller exchange repulsion envelope at the O4 terminus. Therefore, the electronegative end of the 1,3-dipole can approach the dipolarophile closer. This effect is significant for 1,3-dipoles such as **1**, **3**, or **4** that have different electronegativities for their terminal groups.

As the reactants approach each other, the 1,3-dipole polarizes the incoming dipolarophile. For the discussion of the polarization effects, the geometry at the first point of the last prechemical phase (denoted as **C** in Figure 3a−j) is used, where the z-axis was chosen as the ethene C−C axis, and the x-axis is in the plane of ethene perpendicular to the z-axis. In this frame, the dipole-induced dipole interaction of the reactants depends on the dipole moment of the 1,3-dipole $\mu_z^{1,3}$ along the z axis, which in the case of **4** is with 3.0 D (Table 3) relatively large as is also the polarizability of the 1,3-dipole in z-direction (5.1 Å^3, Table 3). These values must be compared with the polarizability of ethene (α_{iso}: 3.00 Å^3), which is substantially larger than that of acetylene (2.18 Å^3, Table 4). Hence, the 1,3-dipole polarizes ethene stronger than acetylene, lowering the barrier of the former. Clearly, the approach of the reactants in the chemical phases is facilitated because mutual attraction is enlarged by the larger ethene polarizability and the enlarged induced dipole moment.

The comparison of the polarizabilities and dipole moments listed in Table 3 reveals that each 1,3-dipole should react differently and that the close agreement with regard to the reaction barriers of two different dipolarophiles (Table 4) seems to be accidental and cannot be simply correlated to some property of the reactants. For example, reactions **4** and **7** are comparable insofar as they both approach with their oxygen end first atom C1 and polarize with their relatively large dipole moment the π-density, so that C1 becomes partially positively charged and C3 partially negatively charged. In the coplanarization phase, the large orientation angles of 34.2 and 27.5°, respectively, must be decreased, which costs energy and explains the relatively large contributions to the acetylene barrier in this phase.

However, the actual increase in the barrier is based on the bending and rehybridization phase, which is the first chemical phase. The prerequisite for rehybridization is the transfer of charge from the 1,3-dipole to the dipolarophile. Such a charge transfer requires a nucleophilic 1,3-dipole with a high-lying LUMO (**3**, **6**, **8**, and **9** in Figure 1), whereas the electrophilic
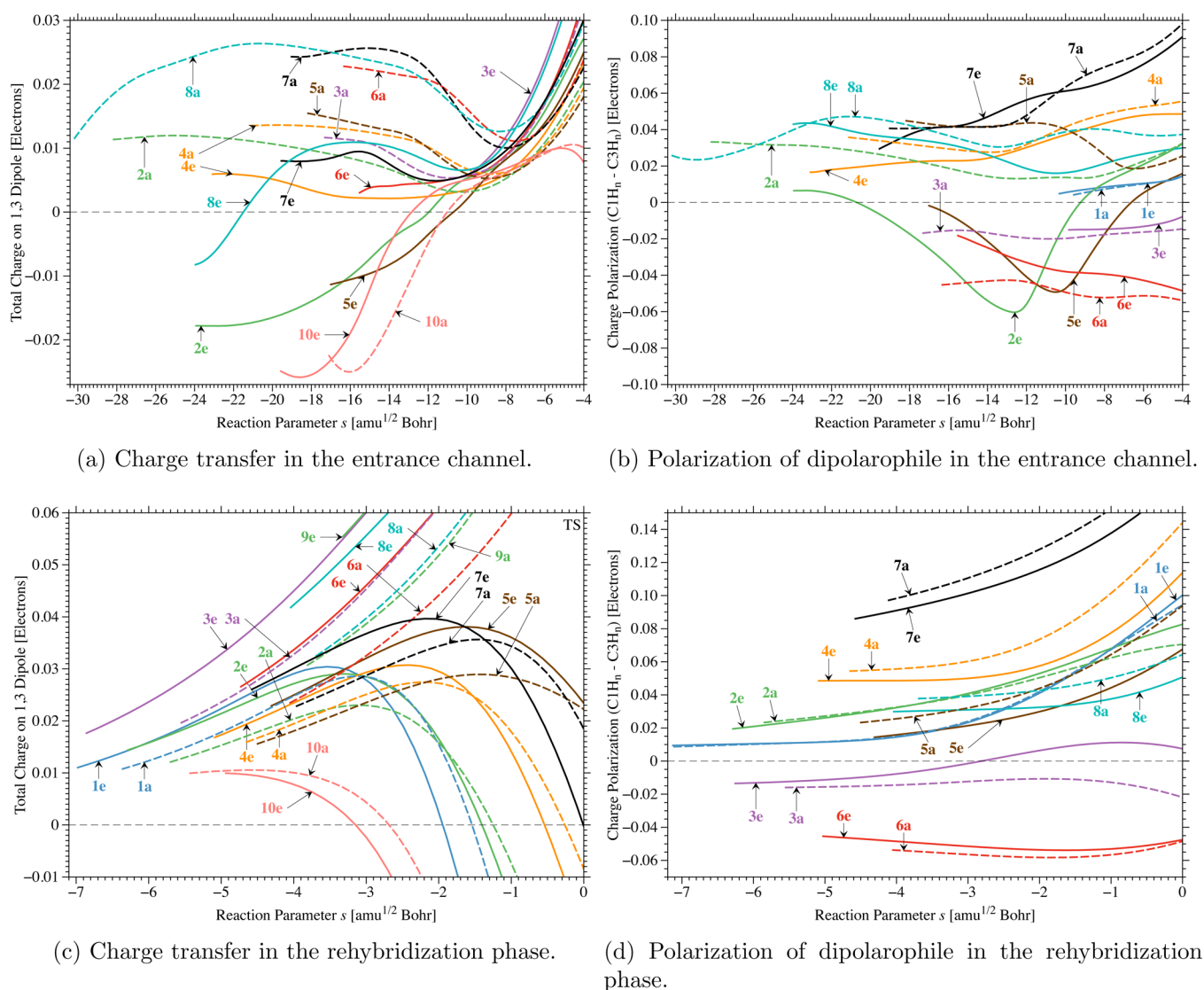
(a) Charge transfer in the entrance channel.

(b) Polarization of dipolarophile in the entrance channel.

(c) Charge transfer in the rehybridization phase.

(d) Polarization of dipolarophile in the rehybridization phase.

Figure 4. (a) Charge transfer from the 1,3-dipole to the dipolarophile (indicated by positive values) in the entrance channel given as a function of the reaction parameter s. Solid lines: ethene; dashed lines: acetylene. (b) Charge polarization of the dipolarophile (calculated as the difference in charges q: $q(C1H_n) - q(C3H_n)$; positive values indicate that C3 has become more negatively charged) in the entrance channel given as a function of the reaction parameter s. (c): Same as (a), but with curves trimmed to begin at the rehybridization phase. (d) Same as (b), but with curves trimmed to begin at the rehybridization phase. (TS always at $s = 0$ amu$^{1/2}$ bohr) B3LYP/6-31G(d,p) calculations.

1,3-dipole in **1**, or the amphiphilic 1,3-dipoles **2**, **5**, and **7**, are less suitable for such a charge transfer according to frontier molecular orbital (FMO) theory and the energies of HOMO and LUMO. In this situation, it is of advantage to analyze the actual charge transfer values as obtained from an NBO analysis and compared for the first time for all 20 reactions investigated on a one-to-one basis as shown in Figure 4. Such a comparison is only possible by URVA, as it requires an accurate description of the reaction valley far out into the entrance channel[80] and the use of mass-weighted coordinates. Figure 4 reveals that the charge transfer and charge polarization situation is much more complex, as it can be anticipated by an investigation of the TS via FMO theory.

For the majority of the reactions investigated, charge transfer from the 1,3-dipole to the dipolarophile takes place throughout the entrance channel and is stronger and earlier in the case of the ethene reactions, which is in line with the fact that the ethene LUMO is lower in energy (Table 4). In several cases, the 1,3-dipole accepts charge from the dipolarophile (**2e**, **5e**, **8e**, **10e**, **10a**, Figure 4a). Between −10 and −8 s units (where the

coplanarization phase begins), there is a switch in the charge transfer so that the dipolarophile (1,3-dipole) increasingly accepts (looses) negative charge. Nucleophilic 1,3-dipoles are stronger charge donors (**3** ≈ **9** > **8** > **6** in Figure 4c) than amphiphilic or electrophilic 1,3-dipoles (**1** > **10**) that are first donors but become acceptors up to 3 s units before the TS (Figure 4c). Apart from this, the donor ability is always larger in connection with dipolarophile ethene than acetylene (Figure 4c).

Although the charge transfer from the 1,3-dipole to acetylene is smaller than that to ethene (in line with the values of HOMO and LUMO, Table 4) at a given s before the rehybridization phase, the polarization of the C1C3 bond is always stronger for acetylene than ethene (even when it is inverted as for **3** or **6**; Figure 4d). This is a result of the high-lying LUMO of acetylene, which facilitates charge polarization. This implies that a charge transfer to this LUMO is more effective than that to the ethene LUMO, and even though it might be delayed and smaller (Figure 4a) the resulting charge polarization, which facilitates the cycloaddition, is more effective for the acetylene reactions

(Figure 4d). This is an unexpected result and confirms that a description of the 1,3-dipolar cycloadditions in terms of FMO theory is a too simple and perhaps even misleading description. In passing we note that Figure 4 provides a quantitative differentiation between nucleophilic, electrophilic, and amphiphilic 1,3-dipoles.

The charge polarization is decisive for the bending of the CCH unit or the pyramidalization of a CCH_2 group. These processes cost energy, and therefore the energy requirement of the bending and rehybridization phase predominates the magnitude of the reaction barrier. This is illustrated in Figure 5 that reveals that
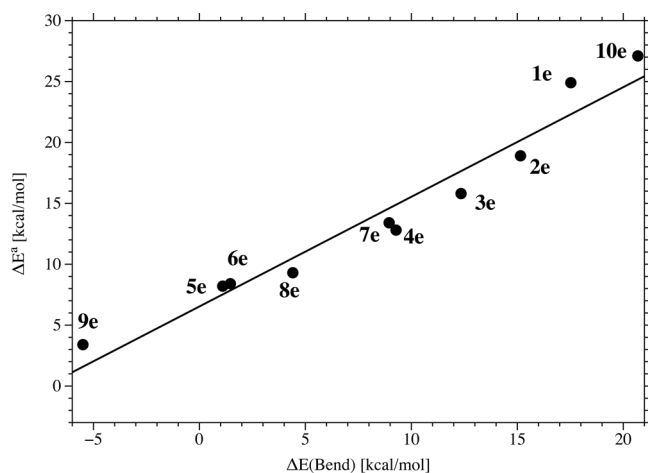

Figure 5. Correlation between activation barrier ΔE^a and energy change during bending phase ΔE(bend) for reactions with ethene. ΔE(bend) is negative for **9** because the bending phase extends far after the TS for this reaction. B3LYP/6-31G(d,p) calculations.

ΔE(bend) and the activation energy ΔE^a (Table 2) are related: A small (large) barrier value implies a small (large) ΔE(bend) value. Deviations from the linear relationship shown in Figure 5 result from contributions in the prechemical phases. The values for the diazonium betaines are larger than those for the nitrilium betaines, where the latter are comparable to those of the azomethines.

Chemical Phases. There are three chemical phases, which are indicated in Figure 3 by a gray horizontal bar. The first of these phases precedes (or even contains) the TS and therefore must be discussed in detail.

Rehybridization and Bending Phase. Charge transfer to the dipolarophile leads to a population of antibonding orbitals and by this to a distortion of its planar (linear) geometry, where charge polarization facilitates this process. This in turn is the prerequisite for forming (bi)radicaloids, which initiate the bond-forming processes. Any loss of charge reduces 4π-electron delocalization in the 1,3-dipoles, weakens the multiple bonds of the XYZ unit, and thereby prepares it for bending and the formation of a biradicaloid. The bending of the 1,3-dipole leads to a switch in the approach modes between 1,3-dipole and dipolarophile, which can be demonstrated for reaction **4**. In the orientation phase, the distance C1O4 is always smaller than the distance C2C3. Charge transfer to the dipolarophile and the closer contact with O4 are responsible for the fact that the C1C3 bond density is polarized toward C3. Accordingly, pyramidalization (bending) and subsequent radicaloid formation is facilitated at C3. Loss of charge is largest at C2 of the 1,3-dipole so that with the bending of the 1,3-dipole also the bending of the H10C2N5 unit and radicaloid formation at C2 starts.

First Bond-Formation Phase. Once radicaloid centers have been formed in the two reactants, the two most advanced ones form the first bond. In reaction **4**, these are C3 and C2; that is, the distance between these atoms is rapidly reduced. In all cases, the less electronegative terminus of the 1,3-dipole forms the first bond to ethene (acetylene), even though the approach between these centers is delayed in the prechemical phases of the reaction. Typically, the corresponding curvature peaks is broad and small and in some cases just a shoulder of the following much larger curvature peak (e.g., **1e**, **2e**, **6e**, **8e**, **9e**, **10e**; Figure 3), which indicates that the process strongly depends on the stepwise pyramidalization and polarization of the CH_2 center involved in the first bond formation and the coupling of these changes with the rehybridization process at the second C atom involved. The stronger this coupling is, the smaller the reaction barrier becomes (for exceptions, see the diazonium betaines).

Second Bond-Formation Phase. In the final phase of the ethene reactions, the second bond is formed, and the RC adopts (with the exception of **1e**, which leads to a planar product) the form of a puckered five-membered ring of specific pseudorotation phase, which is given in Figure 1. Products, which contain a double bond, form an envelope conformation with a phase angle close to $\phi_2 = 72°$ (**2e−6e**, Figure 1), whereas those systems leading to a saturated five-membered ring prefer either an envelope form at $\phi_2 = 180°$ (**9e**, **10e**) or a twist form close to $\phi_2 = 198°$ (**7e**, **8e**).

Since the second C atom has already been prepared and rehybridized in the previous phase, the formation of the second bond is rapid and leads to a high curvature peak. The fact that many internal coordinate components contribute to this peak reveals that bond formation and the conformational/configurational relaxation happen in this phase rapidly, which in view of the relatively large energy release is understandable. In symmetric or nearly symmetric systems, both bonds are formed simultaneously in the second bond-formation phase. In none of the reactions, a postchemical phase occurs, because with the bond formation and the energy set free the RC rapidly adopts its final conformation (Figure 3).

4. COMPARISON OF THE CYCLOADDITION MECHANISMS OF THE TWO DIPOLARPHILES

Although all reactions seem to have a similar overall mechanism in the chemical phases, there are noticeable differences related to orientation, charge transfer, symmetry adjustment, energy release, and product relaxation. As pointed out above, for many RCs intermolecular hydrogen interactions play a key role and lead to the larger stability of the acetylene van der Waals complexes. This we verified by calculating the strength of these interactions with the help of the local H···X stretching force constants.[108,109] For each reacting system, the van der Waals complex determined in the entrance channel (or an equivalent path point) was taken as a reference. Local mode force constants were determined for all intermolecular interactions within the van der Waals distance. Assuming that the energy required to break an H···X interaction is proportional to the H···X local stretching force constant,[110] the sum of H···X force constants should provide a qualitative measure for the total energy cost in the prechemical phases.

Figure 6 reveals that there is a qualitative relationship between the energy cost of the prechemical phases and the sum of the local stretching force constants of the H···X interactions that must be cleaved to obtain coplanarity for the two reactants. Excluded from this correlation are RCs with no initial H···X
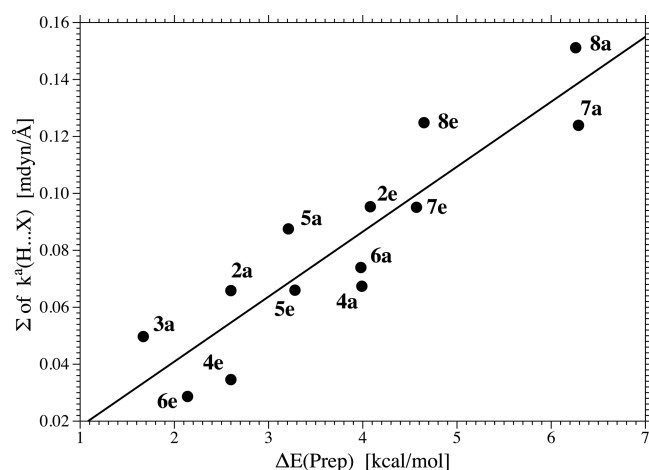
Figure 6. Correlation between the sum of the local force constants $k^a(H\cdots X)$ for $H\cdots X$ interactions in the van der Waals complexes (Figure 2) and the energy cost $\Delta E(prep)$ for the prechemical orientation phases (Table 2). The correlation is positive; that is, larger force constants imply more costly prechemical reorganization (the cost of breaking a $H\cdots X$ interaction is 43.83 kcal mol^{-1}/mdyn/Å; $R^2 = 0.81$). The y-intercept is small. See Supporting Information for individual local force constants. B3LYP/6-31G(d,p) calculations.

Figure 7. Comparison of the curvature and curvature components (N5: C2N5O4 bending; C1: pyramidalization at the C1 atom; C3: pyramidalization at the C3 atom) for reactions **4a** and **4e**. For this reaction, the N5 curvature peak for **4a** occurs at $s = -3.00$, the C3 peak at $s = -2.55$ s units. The peak offset for **4a** is -0.45 s units. The N5 curvature peak for **4e** occurs at $s = -2.94$, the C3 peak at $s = -1.26$ s units. The peak offset for ethene reaction is greater, at -1.68 s units. See Table 5, for the offsets of all reactions. The sudden change in the C1 acetylene component at -0.5 s units results from a trans–cis switch of slightly trans-bent dipolarophile. B3LYP/6-31G(d,p) calculations.

interactions (**1**, **3e**, **9**) and systems where the reaction path in the entrance channel ends at a bifurcation point B (**10**). Force constants used in the correlation are given in the Supporting Information. For all reactions where H-bonds or H-π interactions are present, the energy cost of the prechemical phases correlates well with the strength of these interactions, as measured by the local mode force constants. With a few exceptions, results are in line with the observation that van der Waals complexes between the 1,3-dipole and acetylene are stronger. These differences lead to a different prechemical reaction mechanism.

These differences are best clarified by the charge transfer diagram in Figure 4a, which includes changes in the prechemical phases. The charge transfer to the dipolarophile is always stronger and mostly earlier for the acetylene reactions facilitated by the H interactions. Values are small (5−25 millielectron) but essential for a labilization of the linear geometry of acetylene: Occupation of any of its antibonding orbitals facilitates a bending of the HCC units. This leads to a lowering of the acetylene LUMO and by this improves its electron-acceptor ability. An obvious exception is observed for 1,3-dipole **10** that as a strong electrophilic molecule, accepts charge from the dipolarophile, where **10e** is ahead of **10a**. Figure 4a also reveals that, with the transition from the prechemical to the chemical phases, there is a minimum and/or switch in charge transfer, with the result that ethene becomes the dipolarophile and the stronger charge acceptor. In summary, Figure 4a, in a condensed form, provides insight into the differences between the acetylene and ethene reactions. In most of the cases, acetylene can form end-on complexes with the 1,3-dipole and facilitate in this way an early charge tranfer to the dipolarophile, which is absolutely necessary for a labilization of its linear geometry and a lowering of its LUMO to guarantee that acetylene can act as an efficient charge acceptor in the first chemical phase (bending and rehybridization). For this purpose, it must rotate into another position, which cleaves the H interactions, reduces the charge transfer (minima in Figure 4a), and therefore costs energy. However, the actual purpose of the prechemical phases (preparation for the
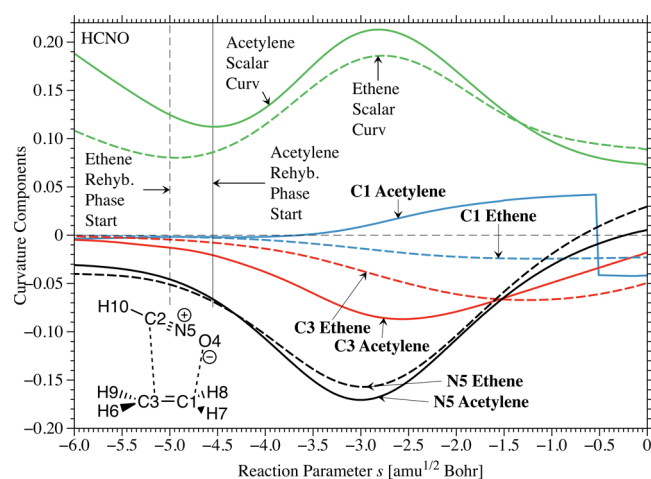
actual cycloaddition) is accomplished. We come to the stunning conclusion that *the fate of the RC is already determined far out in the entrance channel.*

Comparison of the chemical phases of the acetylene and ethene cycloadditions. In Figure 7, the bending and rehybridization phases of **4a** and **4e** are compared. The curvature maxima and by this the maxima of electronic reorganization occur at the same positions (entrance channel, −2.8 s units). The bending of the 1,3-dipole (here C2N5O4 bending; abbreviated in Figure 7 as *N5 Ethene* or *N5 Acetylene*) precedes the bending/pyramidalization at C3, which leads to the C3C2 bond formation. Bending of HC3C1 in acetylene (*C3 Acetylene*) is clearly ahead of the pyramidalization of H$_2$C3C1 in ethene (*C3 Ethene*, Figure 7) as is indicated by the corresponding C3 component minima (the RC resists bending). Once bending/pyramidalization starts at C3 (C1), a similar process is initiated at the neighboring C1 (C3) atom, where again the C1 (C3) of acetylene is somewhat ahead of the C1 (C3) of ethene (Figure 7).

One can quantify the change in rehybridization due to bending/pyramidalization by focusing on the central atom Y = N5 of the 1,3-dipole and that carbon atom (C3 or C1) that undergoes the first bond formation with a terminal atom of the 1,3-dipole. The degree of rehybridization is given for these atoms (groups) by the expression $\eta s = 100(\tau(max) - \tau(s))/\tau(max)$, where $\tau(max)$ is the bending/pyramidalization angle in the final product and $\tau(s)$ is the value at a given path point s. Since 20 reactions and in each reaction up to five groups were investigated, it turned out to be useful to focus just on N5 and C3 (C1) and consider the differences $\Delta\eta(s)$ between acetylene and ethene $(\Delta X\eta(s) = \eta(e, s) - \eta(a,s))$ thus leading to 20 different curves $\Delta\eta(s)$ that are all shown in Figure 8. In addition, the shift Δs of the curvature maximum of the rehybridization phase (that is closely related to the bending at N5; see Figures 3 and 7) into the entrance channel relative to the minimum of the C3 (or C1) bending/pyramidalization component is given for the acetylene and ethene reactions in Table 5.
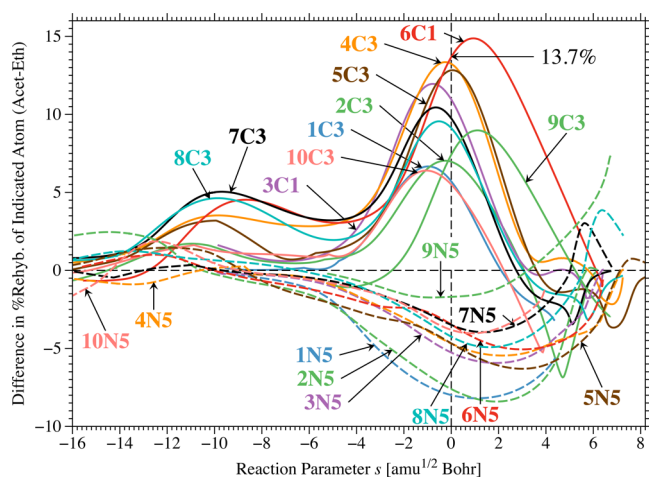
Figure 8. Differences in the rehybridization (given in %) of the reactants in reactions **1**−**10** when the dipolarophile acetylene is replaced by ethene. For example, C1 is the most advanced dipolarophile atom in reaction **6**. At the TS, C1(a) is 36.3% rehybridized, whereas C1(e) is just 22.6% rehybridized. The difference between these numbers, C1(a) − C1(e) = 13.7%, is shown in the graph. Similar calculations are done for the most advanced dipolarophile terminus for each reaction, and for the central N5 atom of the 1,3-dipole. B3LYP/6-31G(d,p) calculations.

Both Figure 8 and Table 5 reveal that, for reactions **1**−**6**, the 1,3-dipole bending peak occurs as in reaction **4** before the first dipolarophile rehybridization peak (Figure 3). For **7a**−**10a** (the azomethines and nitryl hydride), the first acetylene rehybridization peak is found before the 1,3-dipole bending peak.[77] For reactions **7e**−**10e**, the 1,3-dipole bending peak is again before the first ethene bending peak (Figure 3). However, for all reactions, acetylene rehybridization occurs earlier than ethene rehybridization, thus underlining that acetylene is easier to rehybridize than ethene. As pointed out in the previous section, this is due to a higher-lying LUMO that, once populated in the prechemical phases with the charge transferred from the 1,3-dipole, effectively triggers rehybridization (bending) of acetylene. The calculated Δs values (Table 5) are 1 ± 0.2 s units, but vary from 0.45 to 1.74 for **8**−**10**. In the latter cases, the RC has either to undergo complicated rotations (e.g., **8**) or similar movements (e.g., **9**). Exact s and Δs values for all reactions are tabulated in the Supporting Information.

As shown in Table 4, ethene is more polarizable than acetylene, both in z-direction (along the CC bond; Figure in Table 4) and y-direction (π-direction). The larger polarizability of ethene gives the dipolarophile a better chance of responding to the 1,3-dipole and thereby forming more easily a (bi)radicaloid. In the moment, the (bi)radicaloid is formed, the polarizability of the RC shown in Figure 9a must be at its maximum. This is after rather than before the TS (Figure 9a), as the TS is in all cases early, and the (bi)radicaloid formation and bond formation take place in the second chemical phase, that is, after the TS. The polarizability maximum is always larger for ethene than for acetylene (Figure 9b) in line with the data given in Table 4. The larger polarizability maximum for the ethene reaction correlates with the lower reaction barrier for this dipolarophile. The deviations in the barrier value should be and are small, as the differences in polarizability between ethene and acetylene RCs are similar for the 10 1,3-dipoles investigated. The difference in α_{iso} narrows down to values between 0.75 and 0.85 Å³ for all 1,3-dipoles at the transition state. (Figure 9b). In the saturated products with no double bond the isotropic polarizability adopts

a minimum value when the second bond is formed (**8**−**10**) or just an intermediate minimum when the formation of a double bond leads to some variation in $\Delta\alpha_{iso}(s)$.

The dipole moments $\mu(s)$ of the various RCs are rather steady in the prechemical regions (Figure 9d). Their magnitudes and changes are directly related to the strength of the H-interactions and the configuration of the H-bonded van der Waals complexes, which implies larger total dipole moments $\mu(s)$ for acetylene as a dipolarophile. A more complex pattern of the changes in $\mu(s)$ results for the chemical regions before and after the TS (Figure 9c). Common to all reactions is a decrease of $\mu(s)$ before or after the TS in the region where the (bi)radicaloids are formed and an increase of $\mu(s)$ when a puckered five-membered ring with heteroatoms (and a double bond) leads to a permanent dipole moment (Figure 9c). The decrease in $\mu(s)$ underlines that zwitterionic structures that are often discussed by organic chemists in connection with the reaction mechanism of 1,3-dipolar cycloadditions do not play any role for most of the reactions as the mechanism proceeds via (bi)radicaloid transient forms. An exception may be **1**, where a strong increase of $\mu(s)$ takes already place in the bending phase before the TS (blue lines in Figure 9c).

The difference in the rehybridization of C3 (C1) and C1 (C3) can be used to define the asynchronicity of the two bond-forming processes after the TS (given in Table 5 in percentage). Clearly, the asynchronicity of the acetylene reactions is larger in line with the larger exothermicity of these reactions compared to their ethene analogues (Table 1). Within a given group of 1,3-dipoles, that reaction has the larger asynchronicity that involves a 1,3-dipole with the larger electronegativity difference $\chi(X) - \chi(Z)$, because this implies a larger polarization of the dipolarophile and in consequence a much earlier formation of the first bond compared to that of the second bond. Charge transfer leads to a larger polarization of acetylene (Figure 4c) and an earlier rehybridization, so that the asynchronicity is larger for the acetylene reaction.

RC **3** also has a large asynchronicity because the N terminus is substantially more electronegative than the C terminus, and the dipolarophile is significantly polarized. For RCs **3** and **6**, the X2 terminus of the 1,3-dipole is more electronegative than its Z4 terminus, so that the asynchronicity adopts negative values. The smallest asynchronicity is obtained for RCs **2** and **6** because $\chi(X) - \chi(Z)$ adopts in these cases a relatively small value. Noteworthy is that a small asynchronicity not necessarily implies a low barrier (see **2** and **10**). The relative polarizability of X and Z plays also a large role.

The fact that acetylene rehybridizes earlier than ethene, and that acetylene rehybridization is more advanced at the transition state, can be directly related to the LUMO energies (see above) and the local bending and pyramidalization force constants of the dipolarophiles (0.15 vs 1.63 mdyn/Å, Table 4). Bending of acetylene is facilitated, as a pπ orbital can mix with a 1s(H) orbital, thus leading to a new CH bonding orbital. The same happens in the case of ethene; however, with the difference that the pπ−1s overlap is much smaller, and therefore the stabilization of the new CH$_2$ group orbitals is also smaller. This discussion shows that there are opposing effects on the reaction mechanism of a given 1,3-dipole if acetylene is replaced by ethene: differences in the stabilities of the van der Waals complexes formed, the prechemical reaction mechanisms (preparation of the RC for reaction), charge transfer and charge polarization, rehybridization and (bi)radicaloid formation, asynchronicity, and bond formation. Therefore, a simplified analysis
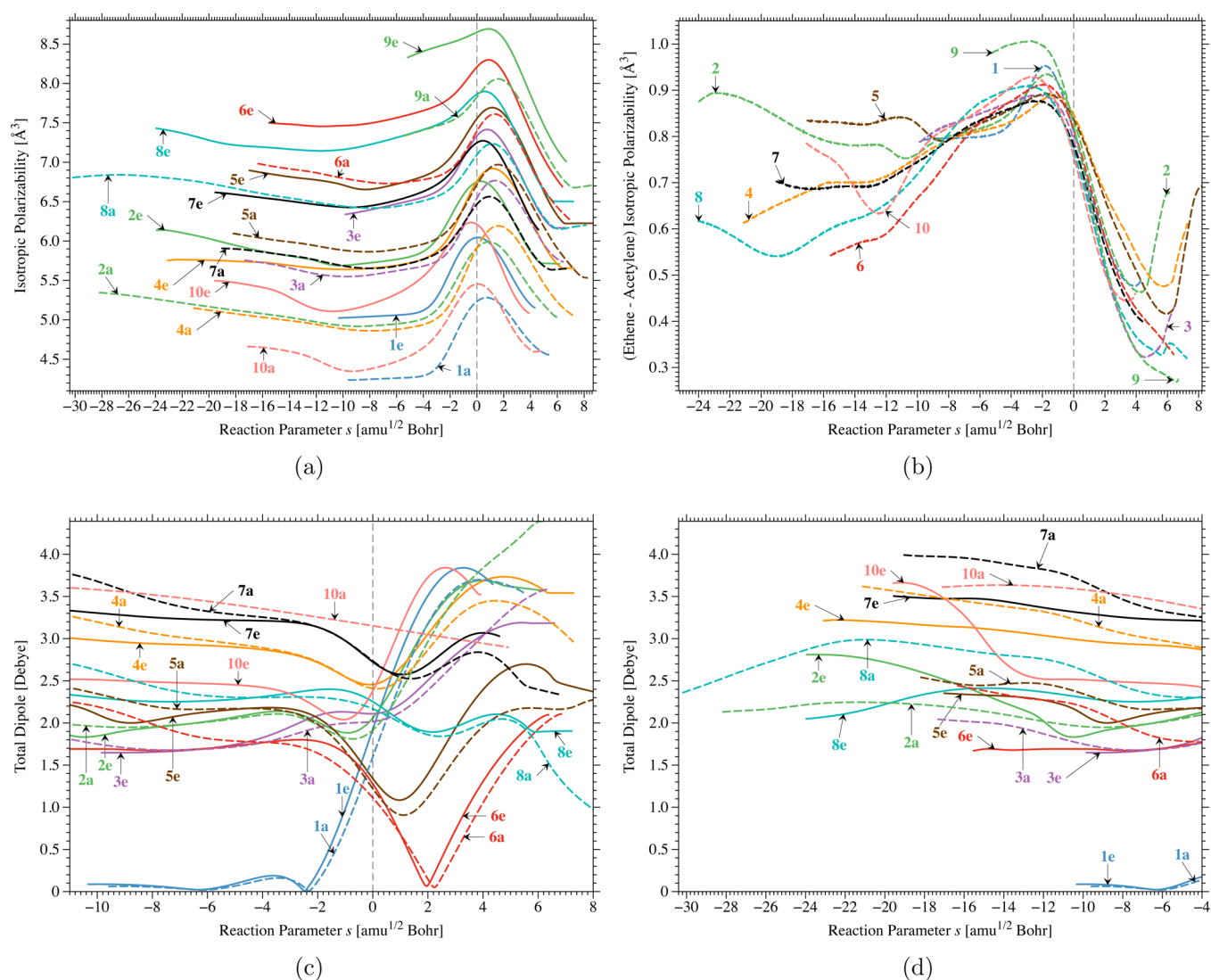
Figure 9. (a) Isotropic polarizability $\alpha_{iso}(s)$ $[\text{Å}^3]$ of the RC as a function of s. (b) Difference in the isotropic polarizabilities, $\Delta\alpha_{iso}(s) = \alpha_{iso}(a, s) - \alpha_{iso}(e, s)$ $[\text{Å}^3]$. (c) Changes in the dipole moment $\mu(s)$ [debye] of the RC in the chemical phases. (d) Changes in the dipole moment $\mu(s)$ [debye] of the RC for the entrance channel. Solid lines denote cycloadditions with e, dashed lines with a. B3LYP/6-31G(d,p) calculations.

of the reaction mechanism by using either orbital, electron density, or energy decomposition models cannot explain the varying features of the 1,3-dipolar cycloadditions.

URVA2016 provides a new methodology of studying chemical reactions as is demonstrated by diagrams like the ones shown in Figure 4: The charge transfer between the reactants is more advanced for the electrophilic and amphiphilic 1,3-dipoles **1**, **2**, and **10** in the case of the acetylene reactions and therefore might contribute to their smaller barriers. In all other cases, charge transfer is earlier for the ethene reactions in line with their lower barriers (Table 1). However, this insight is only possible if one analyzes the changes in charge transfer throughout the entrance channel of the reaction, where the analysis must be guided by the curvature diagrams of Figure 3 to identify the mechanistically relevant reaction phases.

5. CONCLUSIONS AND CHEMICAL RELEVANCE

Although the 1,3-dipolar cycloadditions with ethene have been investigated many times, this is the first in-depth investigation that compares for 10 different 1,3-dipoles the cycloaddition with the dipolarophiles ethene and acetylene. Several investiga-

tions have pointed out that the two sets of reactions have similar barriers and that because of this the mechanism of these cycloadditions should be the same.[47−49,53] Utilizing URVA2016 with its component analysis[6] and a new set of internal coordinates including, besides bond lengths and bond angles, also pyramidalization angles and puckering coordinates, this work has laid a basis for a detailed and comparative study of the mechanisms of groups of chemical reactions. Properties of the RC are given as a function of s (Figures 7, 8, and 9) and compared for 20 reactions, where the accuracy of the reaction path description and the mass-weighting turn out to be essential. In this work, dipole moment, isotropic polarizability, degree of rehybridization, asynchronicity of bond formation, charge transfer, and charge polarization have been compared and analyzed where the comparison has been guided by the curvature diagrams.

Figure 10 summarizes the results of the URVA analyses for the 1,3-dipolar cycloadditions **1**−**10** with acetylene or ethene as dipolarophile. Although the mechanisms for the two dipolarophiles are overall similar considering the three phases in the chemical region, there are significant differences with regard to the van der Waals complex formation (stronger for acetylene

Mechanistic Detail	Acetylene (A)	Ethene (E)
Established fact 1	**more exothermic**	**less exothermic**
Hammond-Leffler postulate	TS should be earlier barrier lower	TS should be later barrier heigher
Established fact 2	**barriers are similar (puzzle)**	

	Pre-chemical phases		
1	Van der Waals interactions (H-bonding)	stronger (higher barrier)	weaker (lower barrier)
2	Preparation of the RC	easier (lowering of barrier)	more difficult (increasing barrier)
3	Summary	compensation of opposing effects leading to a slight barrier increase for **A**	

	Chemical phases		
4	Charge transfer	later/weaker/more efficient	earlier/stronger
			exceptions: **1, 2, 10**
5	Charge polarization	larger (higher LUMO)	smaller
6	Bending of 1,3-dipole	later	earlier
7	Rehybridization of dipolarophile	easier	more difficult
8	(Bi)radicaloid formation	dipolarophile first (**"dipolarphile-driven"**)	1,3-dipole first (**"dipole-driven"**)
9	Asynchronicity of bond formation	larger	smaller
10	Summary	4 and 5 are cooperative effects that lead to 7 and 8:	
	Solution of puzzle	**As the ethene reaction is dipole-driven, the difficult step (rehybridization of the dipolarophile) is shifted beyond the TS thus lowering the barrier.**	
		3 + 10 lead to an adjustment of barriers for A and E	

Figure 10. Summary of the results of the URVA analysis for the 20 reactions investigated. See text.

thus raising the barrier) and the RC preparation (easier for acetylene so that in total the barriers for the acetylene reactions are only slightly raised). In the solvent phase, individual H-bonding will be replaced by a multitude of noncovalent effects. Nevertheless, essential mechanistic features of what we find in the gas phase will also play a role in the solvent phase. This will be true for charge transfer and charge polarization, which, although different for the two dipolarophiles (4 and 5 in Figure 10), are cooperative effects that drive the weakening of the π-bonds and the rehybridization of the C atoms of the dipolarophiles (6 in Figure 10) and their conversion into (bi)radicaloids (8 in Figure 10). At least one reaction partner must adopt (bi)radicaloid character to initiate bond formation between 1,3-dipole and dipolarophile. The URVA analysis reveals that in the acetylene reactions the dipolarophile drives the first bond formation, whereas in the ethene reactions the 1,3-dipole takes this role as pyramidalization of the ethene requires more energy.

The major mechanistic difference is that the ethene reactions are *1,3-dipole-driven* in contrast to the acetylene reactions, which are *dipolarophile-driven*. This difference has the result that the energy-demanding rehybridization and pyramidalization of ethene is shifted into the post-TS region, where it becomes possible in the way the RC releases energy. Such a shift is normally found in catalyzed reactions, where the catalyst helps to delay energy-consuming processes so that they cannot determine the barrier height.[111] Hence, one can consider the ethene reactions to be to some extent self-catalyzed (the 1,3-dipole is reaction partner and catalyst at the same time). Several electronic effects (3 and 8 leading to 10, Figure 10) are responsible for the fact that, in spite of the larger exothermicity of the acetylene

reactions, their barriers are comparable to those of the ethene cycloadditions.

Once the difference in the mechanisms of the two dipolarophiles is understood, one can develop recipes to lower the barrier. In a *dipole-driven* reaction, with the generation of a 1,3-biradical destabilized by a suitable Y (e.g., a S atom to facilitate pyramidalization of terminal groups X or Z) a lower barrier results, whereas any electron-donating acetylene substituent helps to lower the barrier of the acetylene reaction.

Apart from this general mechanistic outcome, there are some mechanistic details that are worth mentioning:

(i) The importance of the (bi)radicaloid formation for the cycloaddition is revealed by the fact that the activation barriers correlate with the energy change in the bending/rehybridization phase.

(ii) In the chemical phases, charge transfer from a nucleophilic 1,3-dipole is always toward the dipolarophile. Contrary to the predictions of FMO theory, this is also true for an amphiphilic or electrophilic 1,3-dipole. However, the dipolarophile changes from a donor to an acceptor of negative charge in the bending/rehybridization phase (Figure 4). The direction of charge transfer can be different for different phases.

(iii) The asynchronicity of the two bond formations increases with the electronegativity difference $\chi(X) - \chi(Z)$. Furthermore, it is always larger for the acetylene than for the ethene reactions, as the former is later polarized under the impact of the 1,3-dipole despite its lower isotropic polarizability. For a pair of equivalent reactions, the larger asynchronicity leads to the more exothermic reaction.

(iv) As in the case of the acetylene reactions, the bond with the larger approach distance at the start of the coplanar approach phase is ultimately formed first, which is a result of the fact that the hard sphere Z of the 1,3-dipole polarizes the dipolarophile in a way that is opposite to the charge distribution of the 1,3-dipole. Hence, the C atom next to the less negatively charged X group (atom) of 1,3-dipole XYZ undergoes bond formation first.

(v) Charge transfer assists the rehybridization of both dipole and dipolarophile and is therefore a driving force for the reaction. Electrophilic 1,3-dipoles have a reversal of charge transfer before the TS and consequently higher barriers. Using the charge transfer diagram in Figure 4 the height of the reaction barriers can be anticipated.

(vi) The current investigation reveals shortcomings of the Hammond−Leffler postulate that can no longer be applied in catalytic reactions. Since the ethene reactions can be considered as self-catalyzed, the failure seems plausible.

(vii) It is striking that even for more complicated reaction mechanisms the fate of the RC is largely determined in the van der Waals region.

The results of this work explain why it is in general difficult to correlate properties of the RC with quantities representing the energetics. This can only be done with limited success within a given group of 1,3-dipoles. However, a substituent that changes the nature of X, Y, and Z significantly leads to an unbalancing of the various electronic factors adding to the activation barrier, and accordingly larger or smaller barriers result, which must be analyzed on a case-by-case basis.

■ ASSOCIATED CONTENT

Ⓢ Supporting Information

The Supporting Information is available free of charge on the ACS Publications website at DOI: 10.1021/acs.jpca.6b07975.

Reaction movies (ZIP)

Rehybridization data, local mode force constants, and snapshots of the reaction complex given along the reaction path for all cycloadditions. (PDF)

■ AUTHOR INFORMATION

Corresponding Authors
*E-mail: ekraka.at.smu.edu . Phone: 001-214-768,1609. (E.K.)
*E-mail: dcremer.at.smu.edu. Phone: 001-214-768-1300. (D.C.)

Notes
The authors declare no competing financial interest.

■ ACKNOWLEDGMENTS

■ REFERENCES

(1) Kraka, E.; Cremer, D. Computational Analysis of the Mechanism of Chemical Reactions in Terms of Reaction Phases: Hidden Intermediates and Hidden Transition State. *Acc. Chem. Res.* **2010**, *43*, 591−601.

(2) Cremer, D.; Kraka, E. From Molecular Vibrations to Bonding, Chemical Reactions, and Reaction Mechanism. *Curr. Org. Chem.* **2010**, *14*, 1524−1560.

(3) Konkoli, Z.; Cremer, D.; Kraka, E. Unified Reaction Valley Approach: Mechanism of the Reaction $CH_3 + H_2 \rightarrow CH_4 + H$. *J. Phys. Chem. A* **1997**, *101*, 1742−1757.

(4) Kraka, E. In *Wiley Interdisciplinary Reviews: Computational Molecular Science*; Allen, W., Schreiner, P. R., Eds.; Wiley: New York, 2011; pp 531−556.

(5) Kraka, E. In *Encyclopedia of Computational Chemistry*; Schleyer, P., Allinger, N., Clark, T., Gasteiger, J., Kollman, P., Schaefer, H., III, Schreiner, P., Eds.; Wiley: Chichester, U.K, 1998; Vol. 4; pp 2437−2463.

(6) Zou, W.; Sexton, T.; Kraka, E.; Freindorf, M.; Cremer, D. A New Method for Describing the Mechanism of a Chemical Reaction Based on the Unified Reaction Valley Approach. *J. Chem. Theory Comput.* **2016**, *12*, 650−663.

(7) Sexton, T.; Kraka, E.; Cremer, D. The Extraordinary Mechanism of the Diels-Alder Reaction: Investigation of Stereochemistry, Charge Transfer, Charge Polarization, and Biradicaloid Formation. *J. Phys. Chem. A* **2016**, *120*, 1097−111.

(8) Padwa, A.; Pearson, W. H. *Synthetic Applications of 1,3-Dipolar Cycloaddition Chemistry Toward Heterocycles and Natural Products*; Wiley: New York, 2002.

(9) Nair, V.; Suja, T. D. Intramolecular 1,3-dipolar Cycloaddition Reactions in Targeted Syntheses. *Tetrahedron* **2007**, *63*, 12247−12275.

(10) Padwa, A.; Bur, S. K. The Domino Way to Heterocycles. *Tetrahedron* **2007**, *63*, 5341−5378.

(11) Rane, D.; Sibi, M. Recent Advances in Nitrile Oxide Cycloadditions. Synthesis of Isoxazolines. *Curr. Org. Synth.* **2011**, *8*, 616−627.

(12) Kaur, J. *Azomethines and 1,3 Dipoles - Leading to New Heterocycles: Studies on 1,3 Dipolar Cycloadditions*; LAP LAMBERT Academic Publishing: NewYork, 2011.

(13) Heusgen, R. On the Mechanism of 1,3-Dipolar Cycloadditions. A Reply. *J. Org. Chem.* **1968**, *33*, 2291−2297.

(14) Woodward, R. B.; Hoffmann, R. Die Erhaltung der Orbitalsymmetrie. *Angew. Chem.* **1969**, *81*, 797−870.

(15) Dewar, M. Aromatizitat und Pericyclische Reaktionen. *Angew. Chem.* **1971**, *83*, 859−875.

(16) Nguyen, T. *Frontier Orbitals: A Practical Manual*; Wiley: New York, 2007.

(17) Firestone, R. A. On the Mechanism of 1,3-dipolar Cycloadditions. *J. Org. Chem.* **1968**, *33*, 2285−2290.

(18) Gothelf, K. V.; Jorgensen, K. A. Asymmetric 1,3-Dipolar Cycloaddition Reactions. *Chem. Rev.* **1998**, *98*, 863−909.

(19) Kissane, M.; Maguire, A. Asymmetric 1,3-dipolar Cycloadditions of Acrylamides. *Chem. Soc. Rev.* **2010**, *39*, 845−883.

(20) Xing, Y.; Wang, N.-X. Organocatalytic and Metal-mediated Asymmetric (3 + 2) Cycloaddition Reactions. *Coord. Chem. Rev.* **2012**, *256*, 938−952.

(21) Amblard, F.; Cho, J. H.; Schinazi, R. F. Cu(I)-Catalyzed Huisgen Azide-Alkyne 1,3-Dipolar Cycloaddition Reaction in Nucleoside, Nucleotide, and Oligonucleotide Chemistry. *Chem. Rev.* **2009**, *109*, 4207−4220.

(22) Naodovic, M.; Yamamoto, H. Asymmetric Silver-Catalyzed Reactions. *Chem. Rev.* **2008**, *108*, 3132−3148.

(23) Stanley, L. M.; Sibi, M. P. Enantioselective Copper-Catalyzed 1,3-Dipolar Cycloadditions. *Chem. Rev.* **2008**, *108*, 2887−2902.

(24) Lutz, J. 1,3-dipolar Cycloadditions of Azides and Alkynes: A Universal Ligation Tool in Polymer and Materials Science. *Angew. Chem., Int. Ed.* **2007**, *46*, 1018−1025.

(25) Tron, G.; Pirali, T.; Billington, R.; Canonico, P.; Sorba, G.; Genazzani, A. Click Chemistry Reactions in Medicinal Chemistry: Applications of the 1,3-dipolar Cycloaddition Between Azides and Alkynes. *Med. Res. Rev.* **2008**, *28*, 278−308.

(26) Jewett, J.; Bertozzi, C. Cu-free Click Cycloaddition Reactions in Chemical Biology. *Chem. Soc. Rev.* **2010**, *39*, 1272−1279.

(27) Pieters, R.; Rijkers, R.; et al. D.T.S. and Liskamp Application of the 1,3-Dipolar Cycloaddition Reaction in Chemical Biology: Approaches Toward Multivalent Carbohydrates and Peptides and Peptide-Based Polymers. *QSAR Comb. Sci.* **2007**, *26*, 1181−1190.

(28) Gold, B.; Dudley, G.; Alabugin, I. Moderating Strain without Sacrificing Reactivity: Design of Fast and Tunable Noncatalyzed Alkyne-Azide Cycloadditions via Stereoelectronically Controlled Transition State Stabilization. *J. Am. Chem. Soc.* **2013**, *135*, 1558−1569.

(29) Barbosa, A.; Monteiro, J. On the Electronic Structure of the Diazomethane Molecule. *Theor. Chem. Acc.* **2012**, *131*, 1297−1323.

(30) Das, T. K.; Salampuria, S.; Banerjee, M. Computational DFT Study of the 1,3-dipolar Cycloadditions of 1-phenylethyl- trans-2-methyl Nitrone to Styrene and 1-phenylethyl Nitrone to Allyl Alcohol. *J. Mol. Struct.: THEOCHEM* **2010**, *959*, 22−29.

(31) Braida, B.; Walter, C.; Engels, B.; Hiberty, P. A Clear Correlation between the Diradical Character of 1,3-dipoles and their Reactivity Toward Ethylene or Acetylene. *J. Am. Chem. Soc.* **2010**, *132*, 7631−7637.

(32) Engels, B.; Christl, M. What Controls the Reactivity of 1,3-dipolar Cycloadditions? *Angew. Chem., Int. Ed.* **2009**, *48*, 7968−7970.

(33) Barnes, G.; Hase, W. L. Bent Out of Shape. *Nat. Chem.* **2009**, *1*, 103−104.

(34) Mladenovic, M.; Elhiyani, M.; Lewerenz, M. Electric and Magnetic Properties of the Four Most Stable CHNO Isomers from ab initio CCSD(T) Studies. *J. Chem. Phys.* **2009**, *131*, 034302.

(35) Mladenovic, M.; Lewerenz, M.; McCarthy, M. C.; Thaddeus, P. Isofulminic Acid, HONC: Ab initio Theory and Microwave Spectroscopy. *J. Chem. Phys.* **2009**, *131*, 174308.

(36) Benchouk, W.; Mekelleche, S. M. Theoretical Analysis of the Regioselectivity of 1,3-dipolar Cycloaddition of C-(methoxycarbonyl)-N-methyl with Methyl Acrylate and Vinyl Acetate. *J. Mol. Struct.: THEOCHEM* **2008**, *852*, 46−53.

(37) Merino, P.; Tejero, T.; Chiacchio, U.; Romeo, G.; Rescifina, A. A DFT Study on the 1,3-dipolar Cycloaddition Reactions of C-(hetaryl) Nitrones with Methyl Acrylate and Vinyl Acetate. *Tetrahedron* **2007**, *63*, 1448−1458.

(38) Sakai, S.; Nguyen, M. T. Theoretical Determination of the Electronic Mechanisms of 1,3-Dipolar Cycloaddition Reactions of Fulminic Acid and Diazomethane. *J. Phys. Chem. A* **2004**, *108*, 9169−9179.

(39) Hiberty, P. C.; Shaik, S. A clear correlation between the diradicl character of 1,3-dipoles and their reactivity toward ethylene or acetylene. *Theor. Chem. Acc.* **2002**, *108*, 255−272.

(40) Nguyen, M. T.; Chandra, A. K.; Sakai, S.; Morokuma, K. Another Look at the Mechanism of the Concerted 1,3-Dipolar Cycloaddition of Fulminic Acid to Acetylene. *J. Org. Chem.* **1999**, *64*, 65−69.

(41) Lopez, S.; Munk, M.; Houk, K. N. Mechanisms and Transition States of 1,3-Dipolar Cycloadditions of Phenyl Azide with Enamines: A Computational Analysis. *J. Org. Chem.* **2013**, *78*, 1576−1582.

(42) Lan, Y.; Wheeler, S. E.; Houk, K. N. Extraordinary Difference in Reactivity of Ozone (OOO) and Sulfur Dioxide (OSO): A Theoretical Study. *J. Chem. Theory Comput.* **2011**, *7*, 2104−2111.

(43) Krenske, E. H.; Houk, K. N.; Holmes, A. B.; Thompson, J. Entropy Versus Tether Strain Effects on Rates of Intramolecular 1,3-dipolar Cycloadditions of N-alkenylnitrones. *Tetrahedron Lett.* **2011**, *52*, 2181−2184.

(44) Lan, Y.; Houk, K. N. Mechanism and Stereoselectivity of the Stepwise 1,3-Dipolar Cycloadditions between a Thiocarbonyl Ylide and Electron-Deficient Dipolarophiles: A Computational Investigation. *J. Am. Chem. Soc.* **2010**, *132*, 17921−17927.

(45) Xu, C.; Doubleday, L.; Houk, K. Dynamics of 1,3-Dipolar Cycloadditions: Energy Partitioning of Reactants and Quantitation of Synchronicity. *J. Am. Chem. Soc.* **2010**, *132*, 3029−3037.

(46) Xu, C.; Doubleday, L.; Houk, K. Dynamics of 1,3-Dipolar Cycloaddition Reactions of Diazonium Betaines to Acetylene and Ethylene: Bending Vibrations Facilitate Reaction. *Angew. Chem., Int. Ed.* **2009**, *48*, 2746−2748.

(47) Schoenebeck, F.; Ess, D. H.; Jones, G. O.; Houk, K. N. Reactivity and Regioselectivity in 1,3-Dipolar Cycloadditions of Azides to Strained Alkynes and Alkenes: A Computational Study. *J. Am. Chem. Soc.* **2009**, *131*, 8121−8133.

(48) Ess, D. H.; Jones, G. O.; Houk, N. K. Transition States of Strain-Promoted Metal-Free Click Chemistry: 1,3-Dipolar Cycloadditions of Phenyl Azide and Cyclooctynes. *Org. Lett.* **2008**, *10*, 1633−1636.

(49) Ess, D. H.; Houk, K. N. Theory of 1,3-Dipolar Cycloadditions - Distortion/Interaction and Frontier Molecular Orbital Models. *J. Am. Chem. Soc.* **2008**, *130*, 10187−10198.

(50) Jones, G. O.; Houk, K. N. Predictions of Substituent Effects in Thermal Azide 1,3-Dipolar Cycloadditions: Implications for Dynamic Combinatorial (Reversible) and Click (Irreversible) Chemistry. *J. Org. Chem.* **2008**, *73*, 1333−1342.

(51) Ess, D. H.; Houk, K. N. Distortion/Interaction Energy Control of 1,3-Dipolar Cycloaddition Reactivity. *J. Am. Chem. Soc.* **2007**, *129*, 10646−10647.

(52) Ess, D. H.; Jones, G. O.; Houk, N. K. Conceptual, Qualitative, and Quantitative Theories of 1,3-Dipolar and Diels-Alder Cycloadditions Used in Synthesis. *Adv. Synth. Catal.* **2006**, *348*, 2337−2361.

(53) Jones, G. O.; Ess, D. H.; Houk, K. N. Activation Energies and Reaction Energetics for 1,3-Dipolar Cycloadditions of Hydrazoic Acid with C-C and C-N Multiple Bonds from High-Accuracy and Density Functional Quantum Mechanical Calculations. *Helv. Chim. Acta* **2005**, *88*, 1702−1710.

(54) Ess, D. H.; Houk, K. N. Activation Energies of Pericyclic Reactions: Performance of DFT, MP2, and CBS-QB3Methods for the Prediction of Activation Barriers and Reaction Energetics of 1,3-Dipolar Cycloadditions, and Revised Activation Enthalpies for a Standard Set of Hydrocarbon Pericyclic Reactions. *J. Phys. Chem. A* **2005**, *109*, 9542−9553.

(55) Jung, M. E.; Min, S.; Houk, K. N.; Ess, D. Synthesis and Relative Stability of 3,5-Diacyl-4,5-dihydro-1H-pyrazoles Prepared by Dipolar Cycloaddition of Enones and α-Diazoketones. *J. Org. Chem.* **2004**, *69*, 9085−9089.

(56) Houk, K. N.; Gonzalez, J.; Li, Y. Pericyclic Reaction Transition States: Passions and Punctilios, 1935−1995. *Acc. Chem. Res.* **1995**, *28*, 81−90.

(57) Walton, M.; Yang, Y.; Hong, X.; Houk, K. N.; Overman, L. Ligand-Controlled Diastereoselective 1,3-Dipolar Cycloadditions of Azomethine Ylides with Methacrylonitrile. *Org. Lett.* **2015**, *17*, 6166−6169.

(58) Yang, Y.; Liang, Y.; Liu, F.; Houk, K. N. Diels-Alder Reactivities of Benzene, Pyridine, and Di-, Tri-, and Tetrazines: The Roles of Geometrical Distortions and Orbital Interactions. *J. Am. Chem. Soc.* **2016**, *138*, 1660−1667.

(59) Xie, S.; Lopez, S. A.; Ramstrom, O.; Yan, M. D.; Houk, K. N. 1,3-Dipolar Cycloaddition Reactivities of Perfluorinated Aryl Azides with Enamines and Strained Dipolarophiles. *J. Am. Chem. Soc.* **2015**, *137*, 2958−2966.

(60) Lan, Y.; Zou, L.; Cao, Y.; Houk, K. N. Computational Methods To Calculate Accurate Activation and Reaction Energies of 1,3-Dipolar Cycloadditions of 24 1,3-Dipoles. *J. Phys. Chem. A* **2011**, *115*, 13906−13920.

(61) Tantillo, D.; Lee, J. Reaction Mechanisms: Pericyclic Reactions. *Annu. Rep. Prog. Chem., Sect. B: Org. Chem.* **2011**, *107*, 266−286.

(62) Cahill, K. J.; Johnson, R. P. Beyond Frontier Molecular Orbital Theory: A Systematic Electron Transfer Model (ETM) for Polar Bimolecular Organic Reactions. *J. Org. Chem.* **2013**, *78*, 1864−1873.

(63) Domingo, L.; Picher, T. A DFT Study of the Huisgen 1,3-dipolar Cycloaddition Between Hindered Thiocarbonyl Ylides and Tetracyanoethylene. *Tetrahedron* **2004**, *60*, 5053−5058.

(64) de Cozar, A.; Cossio, F. P. Stereocontrolled (3 + 2) Cycloadditions between Azomethine Ylides and Dipolarophiles: A Fruitful Interplay between Theory and Experiment. *Phys. Chem. Chem. Phys.* **2011**, *13*, 10858−10868.

(65) Domingo, L. R.; Emamian, S. R. Understanding the Mechanism of [3 + 2] Cycloaddition Reactions. The Pseudoradical versus the Zwitterionic Mechanism. *Tetrahedron* **2014**, *70*, 1267−1273.

(66) Domingo, L. R.; Aurell, M. J.; Perez, P. A DFT analysis of the Participation of Zwitterionic TACs in Polar [3 + 2] Cycloaddition Reactions. *Tetrahedron* **2014**, *70*, 4519−4525.

(67) Domingo, L. R.; Aurell, M. J.; Perez, P. A Mechanistic Study of the Participation of Azomethine Ylides and Carbonyl Ylides in [3 + 2] Cycloaddition Reactions. *Tetrahedron* **2015**, *71*, 1050−1057.

(68) Hunt, W. J.; Goddard, W. A. Excited states of H_2O using improved virtual orbitals. *Chem. Phys. Lett.* **1969**, *3*, 414−418.

(69) Bickelhaupt, F. M.; Baerends, E. The case for steric repulsion causing the staggered conformation of ethane. *Angew. Chem., Int. Ed.* **2003**, *42*, 4183−4188.

(70) Kraka, E.; Zou, W.; Freindorf, M.; Cremer, D. Energetics and Mechanism of the Hydrogenation of XHn for Group IV to Group VII Elements X. *J. Chem. Theory Comput.* **2012**, *8*, 4931−4943.

(71) Kraka, E.; Joo, H.; Cremer, D. A Stunning Example for a Spontaneous Reaction with a Complex Mechanism: The Vinylidene-acetylene Cycloaddition Reaction. *Mol. Phys.* **2010**, *108*, 2667−2685.

(72) Kraka, E.; Wu, A.; Cremer, D. Mechanism of the Diels-Alder Reaction Studied with the United Reaction Valley Approach: Mechanistic Differences between Symmetry-allowed and Symmetry-forbidden Reactions. *J. Phys. Chem. A* **2003**, *107*, 9008−9021.

(73) Cremer, D.; Wu, A.; Kraka, E. The Mechanism of the Reaction FH + $H_2C=CH_2 \rightarrow H_2C-CFH_3$. Investigation of Hidden Intermediates with the Unified Reaction Valley Approach. *Phys. Chem. Chem. Phys.* **2001**, *3*, 674−687.

(74) Kraka, E.; Cremer, D. Mechanism and dynamics of organic reactions: 1,2-H shift in methylchlorocarbene. *J. Phys. Org. Chem.* **2002**, *15*, 431−447.

(75) Hammond, G. A Correlation of Reaction Rates. *J. Am. Chem. Soc.* **1955**, *77*, 334−338.

(76) Leffler, J. Parameters for the Description of Transition States. *Science* **1953**, *117*, 340−341.

(77) Freindorf, M.; Sexton, T.; Kraka, E.; Cremer, D. The mechanism of the cycloaddition reaction of 1,3-dipole molecules with acetylene: an investigation with the unified reaction valley approach. *Theor. Chem. Acc.* **2014**, *133*, 1−18.

(78) Joo, H.; Kraka, E.; Quapp, W.; Cremer, D. The Mechanism of a Barrierless Reaction: Hidden Transition State and Hidden Intermediate in the Reaction of Methylene with Ethene. *Mol. Phys.* **2007**, *105*, 2697−2717.

(79) Miller, W.; Handy, N.; Adams, J. Reaction path Hamiltonian for polyatomic molecules. *J. Chem. Phys.* **1980**, *72*, 99−112.

(80) Hratchian, H. P.; Kraka, E. Improved Predictor-Corrector Integrators For Evaluating Reaction Path Curvature. *J. Chem. Theory Comput.* **2013**, *9*, 1481−1488.

(81) Cremer, D.; Pople, J. A. A General Definition of Ring Puckering Coordinates. *J. Am. Chem. Soc.* **1975**, *97*, 1354−1358.

(82) Cremer, D. Theoretical Determination of Molecular Structure and Conformation. 11. The Puckering of Oxolanes. *Isr. J. Chem.* **1983**, *23*, 72−84.

(83) Cremer, D.; Szabo, K. J. In *Conformational Behavior of Six-membered Rings;* Juaristi, E., Ed.; VCH Publishers, 1995; pp 59−136.

(84) Cremer, D.; Izotov, D.; Zou, W.; Kraka, E., *RING;* Southern Methodist University: Dallas, TX, 2011.

(85) Raghavachari, K.; Trucks, G. W.; Pople, J. A.; Head-Gordon, M. A Fifth-Order Perturbation Comparison of Electron Correlation Theories. *Chem. Phys. Lett.* **1989**, *157*, 479−483.

(86) Adler, T.; Knizia, G.; Werner, H.-J. A simple and efficient CCSD(T)-F12 approximation. *J. Chem. Phys.* **2007**, *127*, 221106−221110.

(87) Becke, A. D. Density-functional Thermochemistry. III. The role of Exact Exchange. *J. Chem. Phys.* **1993**, *98*, 5648−5652.

(88) Stephens, P. J.; Devlin, F. J.; Chabalowski, C. F.; Frisch, M. J. Ab Initio Calculation of Vibrational Absorption and Circular Dichroism Spectra Using Density Functional Force Fields. *J. Phys. Chem.* **1994**, *98*, 11623−11627.

(89) Gräfenstein, J.; Cremer, D. Can density functional theory describe multi-reference systems? Investigation of carbenes and organic biradicals. *Phys. Chem. Chem. Phys.* **2000**, *2*, 2091−2103.

(90) Polo, V.; Kraka, E.; Cremer, D. Electron correlation and the self-interaction error of density functional theory. *Mol. Phys.* **2002**, *100*, 1771−1790.

(91) Polo, V.; Kraka, E.; Cremer, D. Some thoughts about the stability and reliability of commonly used exchange-correlation functionals - coverage of dynamic and nondynamic correlation effects. *Theor. Chem. Acc.* **2002**, *107*, 291−303.

(92) Cremer, D.; Filatov, M.; Polo, V.; Kraka, E.; Shaik, S. Implicit and explicit coverage of multi-reference effects by density functional theory. *Int. J. Mol. Sci.* **2002**, *3*, 604−638.

(93) Chai, J.-D.; Head-Gordon, M. Long-Range Corrected Hybrid Density Functionals with Damped Atom-Atom Dispersion Corrections. *Phys. Chem. Chem. Phys.* **2008**, *10*, 6615−6620.

(94) Sherrill, C. D.; Takatani, T.; Hohenstein, E. G. An Assessment of Theoretical Methods for Nonbonded Interactions: Comparison to Complete Basis Set Limit Coupled-Cluster Potential Energy Curves for the Benzene Dimer, the Methane Dimer, Benzene−Methane, and Benzene−H_2S. *J. Phys. Chem. A* **2009**, *113*, 10146−10159.

(95) Dunning, T. J. Gaussian Basis Sets for Use in Correlated Molecular Calculations I. The Atoms Boron Through Neon and Hydrogen. *J. Chem. Phys.* **1989**, *90*, 1007−1023.

(96) Reed, A.; Curtiss, L.; Weinhold, F. Intermolecular interactions from a natural bond orbital, donor-acceptor viewpoint. *Chem. Rev.* **1988**, *88*, 899−926.

(97) Weinhold, F.; Landis, C. R. *Valency and Bonding: A Natural Bond Orbital Donor-Acceptor Perspective;* Cambridge U. Press, 2003.

(98) Kraka, E.; Zou, W.; Filatov, M.; Gräfenstein, J.; Gauss, J.; He, Y.; Wu, A.; Konkoli, Z.; He, Z.; Cremer, D. et al. *COLOGNE16;* Southern Methodist University: Dallas, TX, 2016.

(99) Werner, H. J.; Knowles, P. J.; Kniza, G.; Manby, F. R.; Schütz, M.; et al. *MOLPRO*, version 2010.1, a package of ab initio programs; http://www.molpro.net, 2010.

(100) Frisch, M. J.; Trucks, G. W.; Schlegel, H. B.; Scuseria, G. E.; Robb, M. A.; Cheeseman, J. R.; Scalmani, G.; Barone, V.; Mennucci, B.; Petersson, G. A. et al. *Gaussian 09,* Revision C.01; Gaussian, Inc, 2010.

(101) Lias, S.; Bartmess, J.; Liebman, J.; Holmes, J.; Levin, R.; Mallard, W. Ion Energetics Data in *NIST Standard Reference Database Number 69;* Department of Commerce, 2016.

(102) Johnson, R., III. NIST Computational Chemistry Comparison and Benchmark Database, NIST Standard Reference Database Number 101, Release 15b. http://cccbdb.nist.gov/, 2011.

(103) Morao, I.; Lecea, B.; Cossio, F. P. In-Plane Aromaticity in 1,3-Dipolar Cycloadditions. *J. Org. Chem.* **1997**, *62*, 7033−7036.

(104) Cossio, F. P.; Morao, I.; Jiao, H.; Schleyer, P. v. R. In-Plane Aromaticity in 1,3-Dipolar Cycloadditions. Solvent Effects, Selectivity, and Nucleus-Independent Chemical Shifts. *J. Am. Chem. Soc.* **1999**, *121*, 6737−6746.

(105) McIver, J. W., Jr.; Stanton, R. E. Symmetry Selection-Rules for Transition States. *J. Am. Chem. Soc.* **1972**, *94*, 8618−8620.

(106) Stanton, R. E.; McIver, J. W., Jr Group Theoretical Selection-Rules for Transition States of Chemical Reactions. *J. Am. Chem. Soc.* **1975**, *97*, 3632−3646.

(107) Spoerel, U.; Dreizler, H.; Stahl, W.; Kraka, E.; Cremer, D. Intermolecular Forces in van der Waals Complexes between Argon and Aromatic Molecules: Rotational Spectrum and ab Initio Investigation of Isoxazole-Argon. *J. Phys. Chem.* **1996**, *100*, 14298−14309.

(108) Zou, W.; Kalescky, R.; Kraka, E.; Cremer, D. Relating Normal Vibrational Modes to Local Vibrational Modes with the help of an Adiabatic Connection Scheme. *J. Chem. Phys.* **2012**, *137*, 084114.

(109) Konkoli, Z.; Cremer, D. A New Way of Analyzing Vibrational Spectra I. Derivation of Adiabatic Internal Modes. *Int. J. Quantum Chem.* **1998**, *67*, 1−11.

(110) Zou, W.; Cremer, D. C_2 in a Box: Determining its Intrinsic Bond Strength for the $X^1\Sigma_g^+$ Ground State. *Chem. - Eur. J.* **2016**, *22*, 4087−4089.

(111) Castineira Reis, M.; Lopez, C. S.; Kraka, E.; Cremer, D.; Faza, O. N. Rational Design in Catalysis: A Mechanistic Study of β-Hydride Eliminations in Gold(I) and Gold(III) Complexes Based on Features of the Reaction Valley. *Inorg. Chem.* **2016**, *55*, 8636−8645.